

INPUT–LABEL CORRELATION GOVERNS A LINEAR-TO-NONLINEAR TRANSITION IN RANDOM FEATURES UNDER SPIKED COVARIANCE

Samet Demir¹ & Zafer Doğan^{1,2}

¹Machine Learning and Information Processing Group, KUIS AI Center

²Department of Electrical and Electronics Engineering

Koç University, İstanbul, Turkey

{sdemir20, zdogan}@ku.edu.tr

ABSTRACT

Random feature models (RFMs)—two-layer networks with a randomly initialized fixed first layer and a trained linear readout—are among the simplest nonlinear predictors. Prior asymptotic analyses in the proportional high-dimensional regime show that, under isotropic data, RFMs reduce to noisy linear models and offer no advantage over classical linear methods such as ridge regression. Yet RFMs frequently outperform linear baselines on structured real data. We show that this tension is explained by a *correlation-driven phase transition*: under spiked-covariance designs, the interaction between anisotropy and input–label correlation determines whether the RFM behaves as an effectively linear predictor or exhibits genuinely nonlinear gains. Concretely, we establish a universality principle under anisotropy and characterize the RFM generalization error via an equivalent *noisy polynomial* model. The effective degree of this polynomial—equivalently, which Hermite orders of the activation survive—is governed by the strength of input–label correlation, yielding an explicit boundary in the correlation–spike-magnitude plane. Below the boundary, the RFM collapses to a linear surrogate and can underperform strong linear baselines; above it, higher-order terms persist and the RFM achieves a clear nonlinear advantage. Numerical simulations and real-data experiments corroborate the theory and delineate the transition between these two regimes.

1 INTRODUCTION

Random feature models (RFMs) Rahimi & Recht (2007)—two-layer networks with a randomly initialized and fixed first layer and a trained linear readout—are among the simplest nonlinear predictors and a canonical proxy for studying neural-network-style representations without feature learning. A recurring question in modern high-dimensional statistics and learning theory is whether, and when, the nonlinear representation induced by a random first layer yields a *genuine* improvement over classical linear prediction in high dimensions.

A substantial body of recent work provides sharp asymptotic characterizations of RFMs in the *proportional* high-dimensional regime, where the sample size m , dimension n , and width k diverge jointly with fixed ratios. Under *isotropic* covariates, these analyses show that RFMs reduce to appropriately matched *noisy linear* models Montanari et al. (2019); Gerace et al. (2020); Goldt et al. (2022); Mei & Montanari (2022); Hu & Lu (2023), implying that random nonlinear features provide no advantage over linear prediction. Yet RFMs frequently outperform linear baselines on structured real data. This paper explains the tension:

*Under spiked-covariance data, a **correlation-driven phase transition** separates an effectively linear regime from a genuinely nonlinear one. The transition boundary is governed by the anisotropy and input–label correlation.*

Below the boundary, the RFM collapses to a noisy linear predictor and can underperform strong linear baselines; above it, higher-order polynomial terms in the activation persist and the RFM achieves a clear nonlinear advantage. Figure 1a displays this phase diagram in the correlation–spike-magnitude plane.

Random feature regression in the proportional regime We study the standard supervised learning setup with an RFM predictor

$$f_\sigma(\mathbf{x}) = \boldsymbol{\omega}^T \sigma(\mathbf{F}\mathbf{x}), \quad (1)$$

where $\mathbf{x} \in \mathbb{R}^n$ is the input, $\mathbf{F} \in \mathbb{R}^{k \times n}$ is a random feature matrix sampled at initialization and then held fixed, $\sigma : \mathbb{R} \rightarrow \mathbb{R}$ is an activation applied entrywise, and $\boldsymbol{\omega} \in \mathbb{R}^k$ is learned from data. Given training samples $\{(\mathbf{x}_i, y_i)\}_{i=1}^m$, we learn $\boldsymbol{\omega}$ by ridge-regularized least squares,

$$\hat{\boldsymbol{\omega}}_\sigma := \underset{\boldsymbol{\omega} \in \mathbb{R}^k}{\operatorname{argmin}} \frac{1}{m} \sum_{i=1}^m (y_i - \boldsymbol{\omega}^T \sigma(\mathbf{F}\mathbf{x}_i))^2 + \lambda \|\boldsymbol{\omega}\|_2^2, \quad (2)$$

with corresponding training error \mathcal{T}_σ and evaluate performance via the generalization error

$$\mathcal{G}_\sigma := \mathbb{E}_{(\mathbf{x}, y)} (y - \hat{\boldsymbol{\omega}}_\sigma^T \sigma(\mathbf{F}\mathbf{x}))^2. \quad (3)$$

Our focus is the proportional asymptotic limit $m, n, k \rightarrow \infty$ with $n/m, n/k \in (0, \infty)$, which is also called the *linear scaling* regime.

Why isotropic theory predicts “effective linearity” Under isotropic covariates (e.g., $\mathbf{x} \sim \mathcal{N}(0, \mathbf{I}_n)$), RFMs admit a precise asymptotic reduction to a matched noisy linear model Montanari et al. (2019); Gerace et al. (2020); Goldt et al. (2022); Mei & Montanari (2022); Hu & Lu (2023). In particular, the RFM is asymptotically equivalent (in performance) to

$$\boldsymbol{\omega}^T (\mu_0 \mathbf{1} + \mu_1 \mathbf{F}\mathbf{x} + \mu_* \mathbf{z}), \quad (4)$$

where $\mathbf{1}$ is the all-ones vector, $\mathbf{z} \sim \mathcal{N}(0, \mathbf{I}_k)$ is independent noise, and the constants μ_0, μ_1, μ_* depend on σ via $\mu_0 = \mathbb{E}[\sigma(z)]$, $\mu_1 = \mathbb{E}[z\sigma(z)]$, and $\mu_* = \sqrt{\mathbb{E}[\sigma(z)^2] - \mu_0^2 - \mu_1^2}$ for $z \sim \mathcal{N}(0, 1)$. This reduction underpins sharp predictions for training/generalization curves and double-descent behavior across losses, activations, and regularization Dhifallah & Lu (2020); Belkin et al. (2019); Geiger et al. (2020); Mei & Montanari (2022); Wang & Bento (2022); Demir & Dogan (2024); Nakkiran et al. (2021). Crucially, it also implies that, in isotropic settings, random nonlinear features do *not* yield gains beyond an appropriately matched linear predictor—a conclusion that holds regardless of the choice of activation.

Spiked covariance and input–label correlation The isotropic reduction (4) is tightly coupled to rotational symmetry of the input distribution. Real covariates are rarely isotropic; they often exhibit low-dimensional structure, anisotropic variance profiles, and alignments between directions of large variance and directions predictive of the label Facco et al. (2017). We study RFMs under a structured but analytically tractable anisotropic model: spiked-covariance covariates with a single-index nonlinear teacher Johnstone (2001); Baik et al. (2005),

$$\mathbf{x} \sim \mathcal{N}(0, \mathbf{I}_n + \theta \boldsymbol{\gamma} \boldsymbol{\gamma}^T), \quad y := \sigma_* \left(\frac{\boldsymbol{\xi}^T \mathbf{x}}{\sqrt{1 + \theta \alpha^2}} \right), \quad (5)$$

where $\boldsymbol{\gamma} \in \mathbb{R}^n$ is a fixed “spike” direction with $\|\boldsymbol{\gamma}\|_2 = 1$, $\boldsymbol{\xi} \in \mathbb{R}^n$ is a fixed “label” direction with $\|\boldsymbol{\xi}\|_2 = 1$, and $\alpha := \boldsymbol{\gamma}^T \boldsymbol{\xi}$ is the *input–label correlation* (alignment) parameter. The spike magnitude θ scales as $\theta \asymp n^\beta$ for $\beta \in [0, 1/2)$, and the normalization in (5) ensures the teacher input has unit variance. This data model isolates, in the simplest possible form, the interaction between (i) *anisotropy* in the covariates and (ii) *correlation* between the anisotropic direction and the label, which together determine on which side of the phase boundary the RFM operates. This minimal model isolates the mechanism and yields predictions that remain qualitatively robust under real-world data (see Figure 4). Our analysis extends naturally to multi-spike covariance $\Sigma = \mathbf{I}_n + \sum_{r=1}^R \theta_r \boldsymbol{\gamma}_r \boldsymbol{\gamma}_r^T$ with a multi-index teacher $y = \sigma_*(\boldsymbol{\Xi}^T \mathbf{x})$ for $\boldsymbol{\Xi} \in \mathbb{R}^{n \times R}$: the quantity η generalizes to a vector of per-spike correlations, and the phase boundary becomes a surface in the joint $(\alpha_1, \theta_1, \dots, \alpha_R, \theta_R)$ space. We focus on the rank-one case ($R = 1$) throughout, as it already captures the core mechanism—the $\theta\alpha$ amplification in the cross-covariance—while keeping the phase diagram two-dimensional and the exposition transparent.

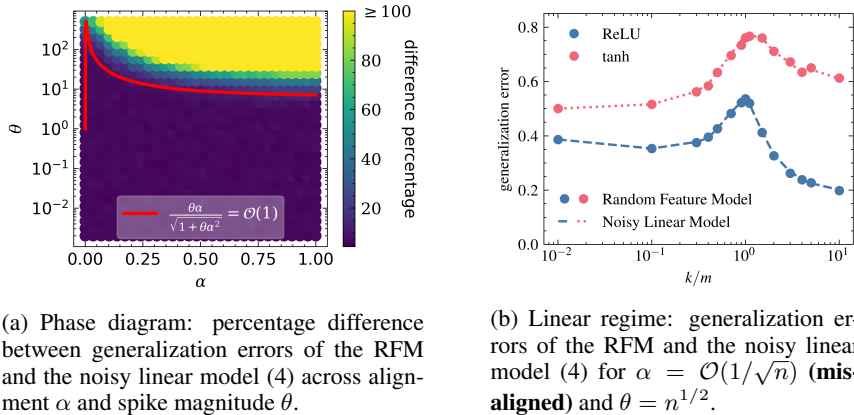


Figure 1: *The phase boundary in the (α, θ) plane.* Left: the red curve separates the effectively linear regime (below) from the genuinely nonlinear regime (above). The red curve marks the phase boundary predicted by Corollary 3. Right: when $\alpha = \mathcal{O}(1/\sqrt{n})$, the RFM lies in the linear regime and matches the noisy linear model across activations. Here $\sigma_* = \sigma_{ReLU}$, $\lambda = 10^{-2}$, $n = 400$, $m = 500$; averages over 50 Monte Carlo runs. Note that we provide our simulation results for the nonlinear regime in Figure 2.

The phase transition and its mechanism Our analysis reveals an explicit transition in the effective nonlinearity of the RFM, controlled by a single quantity η that couples the input–label correlation α , the spike magnitude θ , and the feature matrix \mathbf{F} (see (10)). The mechanism is as follows. The activation σ admits a Hermite expansion whose terms contribute to prediction at different polynomial orders. Under isotropy, all higher-order contributions are suppressed and only the linear term survives—recovering the classical noisy linear surrogate. Under spiked covariance, the quantity η modulates which Hermite orders persist: when $\eta = \mathcal{O}(n^{-1/2})$, only the linear term contributes and the RFM remains effectively linear; when η is larger, higher-order terms activate and the RFM becomes a genuinely nonlinear predictor. The boundary $\eta = \mathcal{O}(n^{-1/2})$ traces an explicit curve in the (α, θ) plane (Figure 1a), cleanly separating the two regimes.

Contributions Our contributions are:

1. **A correlation-driven phase transition in effective nonlinearity.** We identify an explicit boundary in the correlation–spike-magnitude plane that separates an effectively linear regime from a genuinely nonlinear one. Below the boundary, the RFM collapses to the classical noisy linear surrogate and may underperform strong linear baselines; above it, the RFM achieves strictly smaller generalization error through persistent higher-order terms. This provides a data-centric criterion for when random nonlinear features are truly useful in the proportional regime.
2. **Noisy polynomial surrogate with correlation-controlled effective degree.** We characterize the RFM generalization error via an equivalent noisy polynomial model whose degree—equivalently, which Hermite orders of the activation survive—is governed by the input–label correlation. This generalizes the classical noisy linear reduction (4) and makes the role of higher-order effects explicit.
3. **Universality under anisotropy.** As a key technical tool, we establish an activation-level universality theorem under the spiked covariance model: RFM performance depends on the activation only through certain low-order joint moments of $(\sigma(\mathbf{F}\mathbf{x}), y)$. This extends the universality framework of Hu & Lu (2023) beyond isotropic designs.

Our theoretical predictions are supported by experiments, confirming the predicted phase boundary and the transition between effectively linear and genuinely nonlinear behavior.

2 RELATED WORK

Random features, kernels, and linearized network models Random feature models (RFMs) were introduced as randomized approximations to kernel methods Rahimi & Recht (2007). They have since become a canonical object in learning theory, also because RFMs and the Neural Tangent Kernel (NTK) provide complementary linearized viewpoints of two-layer neural networks Ghorbani et al. (2021). Although fully trained networks can empirically outperform both RFMs and NTK predictors Ghorbani et al. (2020), RFMs remain a key testbed for isolating the role of a fixed nonlinear map from that of feature learning.

Proportional-regime asymptotics and noisy-linear equivalence A large literature gives sharp characterizations of RFM training and generalization in the proportional regime under isotropic covariates, via an asymptotic reduction to a matched noisy linear surrogate Montanari et al. (2019); Gerace et al. (2020); Goldt et al. (2020; 2022); Dhifallah & Lu (2020); Mei & Montanari (2022). In particular, Hu & Lu (2023) proves such an equivalence via Lindeberg-type arguments, and Montanari & Saeed (2022) establishes related universality for empirical risk minimization with Gaussian feature replacements. These results underpin precise learning-curve predictions and double-descent analyses Dhifallah & Lu (2020); Mei & Montanari (2022), but they are confined to rotationally invariant data and therefore predict that random nonlinear features offer no advantage over linear prediction. They do not identify structured data settings where this collapse breaks, nor provide an explicit criterion for the transition between linear and nonlinear behavior—the focus of our work.

Beyond isotropy: failures of Gaussian equivalence Recent works show that Gaussian equivalence need not persist under structured data Gerace et al. (2024); Pesce et al. (2023); MAI & Liao (2025), motivating alternative representations such as Gaussian mixtures Dandi et al. (2023b); Demir & Dogan (2025). Our work addresses a complementary question: rather than seeking alternative feature replacements, we characterize *what replaces* the linear surrogate when it breaks under anisotropy. We introduce a concrete noisy-polynomial surrogate for RF regression and show that its *effective degree* (equivalently, which Hermite orders survive) is controlled by input–label correlation, yielding an explicit correlation-driven boundary separating effectively linear and genuinely nonlinear regimes.

Feature learning A parallel line of work studies minimal feature learning via one or few gradient steps, often obtaining improvements over fixed random features Ba et al. (2022); Damian et al. (2022). Ba et al. (2023); Mousavi-Hosseini et al. (2023) analyze sample-complexity benefits under spiked-covariance designs, while Moniri et al. (2024); Dandi et al. (2023a); Cui et al. (2024) characterize the spectral spike induced by gradient updates and establish Gaussian-equivalence statements under isotropic data. Demir & Dogan (2025) extends these Gaussian-equivalence statements to anisotropic mixture data. These analyses exploit data structure through updates to the first layer. Our result is complementary: we show that even without feature learning, anisotropy together with input–label correlation can induce a phase transition in the effective behavior of fixed random features, delineating the baseline that feature-learning methods must improve upon.

Deep random features and alternative scalings Deep random features and anisotropic random layers have been analyzed via precise asymptotics and statistical-physics techniques Schröder et al. (2023); Bosch et al. (2023); Zavatone-Veth & Pehlevan (2023). Complementary work considers polynomial scaling limits Hu et al. (2024); Lu & Yau (2025); Wen et al. (2025), where generalization behavior changes qualitatively with the scaling exponents. These works modify the architecture or scaling regime; in contrast, we keep both fixed and show that data structure alone—anisotropy together with input–label correlation—is sufficient to trigger a linear-to-nonlinear transition in the standard proportional regime.

3 PRELIMINARIES

Notations We denote vectors and matrices using bold letters, with lowercase letters representing vectors and uppercase letters representing matrices. Scalars are indicated by non-bold letters. The notation $\|\mathbf{x}\|_2$ refers to the Euclidean norm of the vector \mathbf{x} while $\|\mathbf{F}\|$ denotes the spectral norm

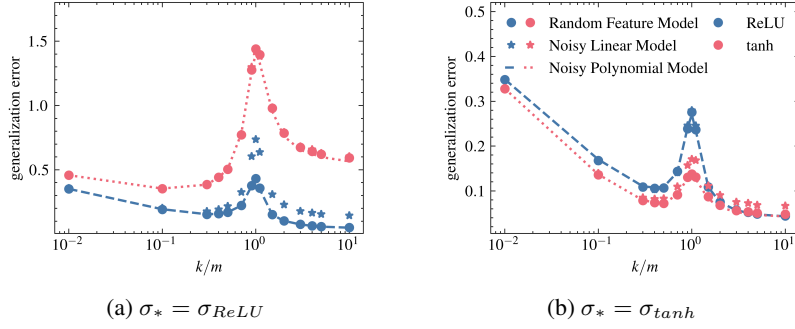


Figure 2: *The nonlinear side of the phase boundary.* When $\alpha = 1$ and $\theta = n^{1/2}$, the RFM crosses the phase boundary and the noisy linear model (4) no longer suffices. The noisy polynomial model (15) captures the RFM generalization error accurately. Here $\lambda = 10^{-3}$, $n = 400$, $m = 500$; averages over 50 Monte Carlo runs.

of the matrix \mathbf{F} . We use the term polylog k to represent any polylogarithmic function of k . The symbol $\xrightarrow{\mathbb{P}}$ indicates convergence in probability. We employ big-O notation, denoted $\mathcal{O}(\cdot)$, and small-o notation, represented as $o(\cdot)$ with respect to the parameters k, n, m . We also use the notation $\theta \asymp n^\beta$ to indicate that there exist constants $C_1, C_2 > 0$ such that $C_1 n^\beta \leq \theta \leq C_2 n^\beta$. Finally, we denote the i -th Hadamard power of a vector \mathbf{x} as $\mathbf{x}^{\odot i}$.

Suppositions We establish our results based on the following assumptions.

- S.1 — The spike and label signal vectors $\boldsymbol{\gamma}, \boldsymbol{\xi} \in \mathbb{R}^n$ are deterministic and $\|\boldsymbol{\gamma}\|_2 = \|\boldsymbol{\xi}\|_2 = 1$.
- S.2 — $\mathbf{x} \sim \mathcal{N}(0, \mathbf{I}_n + \theta \boldsymbol{\gamma} \boldsymbol{\gamma}^T)$ for spike magnitude $\theta \asymp n^\beta$ where $\beta \in [0, 1/2)$.
- S.3 — $y := \sigma_* \left(\frac{\boldsymbol{\xi}^T \mathbf{x}}{\sqrt{1 + \theta \alpha^2}} \right)$ where $\sigma_* : \mathbb{R} \rightarrow \mathbb{R}$ is a function satisfying $|\sigma_*(x)| < C(1 + |x|^K)$ for all $x \in \mathbb{R}$ and some constants $C > 0, K \in \mathbb{Z}^+$.
- S.4 — The number of training samples m , dimension of input vector n and number of intermediate features k jointly diverge: $m, n, k \rightarrow \infty$ with $n/m, n/k \in (0, \infty)$.
- S.5 — $\mathbf{F} := [\mathbf{f}_1, \mathbf{f}_2, \dots, \mathbf{f}_k]^T$ where $\mathbf{f}_i \sim \mathcal{N}(0, \frac{1}{n+\theta} \mathbf{I}_n)$. Note that the covariance of \mathbf{f}_i is selected such that $\mathbb{E}_{\mathbf{x}, \mathbf{f}_i} [(\mathbf{f}_i^T \mathbf{x})^2] = 1$.
- S.6 — The activation function $\sigma : \mathbb{R} \rightarrow \mathbb{R}$ is an odd function satisfying $|\sigma(x)| < C(1 + |x|^K)$ for all $x \in \mathbb{R}$ and some constants $C > 0, K \in \mathbb{Z}^+$.

Discussion of Assumptions S.1–S.3 define the data model. The key parameter is the input–label correlation $\alpha = \boldsymbol{\gamma}^T \boldsymbol{\xi}$, which, together with the spike magnitude θ , controls the phase transition we identify. The restriction $\beta < 1/2$ in S.2 is required by our Lindeberg replacement argument (Appendix A): our concentration bounds regarding $\mathbf{F}\mathbf{x}$ (in Appendix B) fails for $\beta \geq 1/2$. This regime boundary is inherent to the *unconditional* Gaussian equivalence framework used here and in Hu & Lu (2023). Recent *conditional* Gaussian equivalence techniques Dandi et al. (2023a); Demir & Dogan (2025); Wen et al. (2025), which condition on the spike-aligned component of the features rather than treating them monolithically, provide a natural path to extending the analysis to $\beta \geq 1/2$; we expect the phase transition to persist in this regime, as our experiments already confirm (Figure 3c). The normalization in S.3 ensures the teacher input has unit variance, so that label complexity is determined by σ_* alone. S.4 specifies the proportional asymptotic limit. In S.5, the $1/(n + \theta)$ scaling guarantees $\mathbb{E}_{\mathbf{x}, \mathbf{f}_i} [(\mathbf{f}_i^T \mathbf{x})^2] = 1$ regardless of spike magnitude, so that the Hermite expansion of σ —and hence the effective polynomial degree governing the phase transition—is defined with respect to a standard Gaussian argument. S.6 requires σ to be odd with polynomial growth; this is inherited from Hu & Lu (2023) and ensures covariance matching to the linear surrogate (4) via (11). One may drop the odd assumption in the expanse of replacing the linear surrogate with a quadratic one, but it does not affect the phase transition mechanism itself. While ReLU and Softplus violate the

odd-function requirement, all numerical experiments—including those on CIFAR-10 (Figure 4)—confirm that the predicted phase transition persists, suggesting this is a proof artifact rather than a fundamental limitation.

4 MAIN RESULTS

This section develops the theoretical machinery behind the phase transition described in Section 1. We proceed in three steps. First, Section 4.1 establishes a universality theorem under spiked covariance: two activations yield the same RFM performance whenever their low-order moment structures match. Second, Section 4.2 applies this universality to show that every RFM is performance-equivalent to a *noisy polynomial* model whose degree is controlled by the quantity η , which couples input–label correlation, spike magnitude, and feature matrix. Third, Sections 4.3 and 4.4 use this characterization to delineate the two sides of the phase boundary: the effectively linear regime ($\eta = \mathcal{O}(n^{-1/2})$) and the genuinely nonlinear regime (η larger).

4.1 UNIVERSALITY OF RANDOM FEATURES UNDER SPIKED DATA

The classical universality result of Hu & Lu (2023) shows that, under isotropic data, the activation σ can be replaced by a matched Gaussian surrogate (4) without changing training or generalization performance. This result relies on rotational invariance and does not extend to anisotropic settings. The following theorem provides the required extension: under spiked covariance, two activations are performance-equivalent whenever their first two moment structures—covariance and cross-covariance with the label—are matched.

Theorem 1. *Let $\sigma(x)$, $\hat{\sigma}(x)$ be two activation functions satisfying S.6. Suppose that assumptions S.1-S.6 given in Section 3 hold. If*

$$\left\| \mathbb{E}_{\mathbf{x}}[\sigma(\mathbf{F}\mathbf{x})\sigma(\mathbf{F}\mathbf{x})^T] - \mathbb{E}_{\mathbf{x}}[\hat{\sigma}(\mathbf{F}\mathbf{x})\hat{\sigma}(\mathbf{F}\mathbf{x})^T] \right\| = \mathcal{O}(k^{-\varsigma}), \quad (6)$$

$$\left\| \mathbb{E}_{(\mathbf{x},y)}[\sigma(\mathbf{F}\mathbf{x})y] - \mathbb{E}_{(\mathbf{x},y)}[\hat{\sigma}(\mathbf{F}\mathbf{x})y] \right\| = \mathcal{O}(k^{-\varsigma}), \quad (7)$$

are satisfied for some $\varsigma > 0$, then

- (i) the training error \mathcal{T}_σ of the RFM with activation σ , and the training error $\mathcal{T}_{\hat{\sigma}}$ of the RFM with activation $\hat{\sigma}$, both converge in probability to the same value $e_{\mathcal{T}} \geq 0$,
- (ii) the corresponding generalization errors \mathcal{G}_σ and $\mathcal{G}_{\hat{\sigma}}$ also converge in probability to the same value $e_{\mathcal{G}} \geq 0$ under additional assumptions S.7 and S.8 provided in Appendix A.

Proof. The overall strategy follows the Lindeberg replacement method used by Hu & Lu (2023) under isotropy: we define a perturbed training objective, then bound the expected difference when replacing $\sigma(\mathbf{F}\mathbf{x}_i)$ with $\hat{\sigma}(\mathbf{F}\mathbf{x}_i)$ one sample at a time Lindeberg (1922); Korada & Montanari (2011). Extending this argument to spiked covariance requires a new *admissible set* of feature matrices (Appendix B) that controls the spike-projected quantities $|\gamma^T \mathbf{f}_j \mathbf{f}_i^T \gamma|$ and the spectral norm of $\mathbf{F}(\mathbf{I}_n + \theta\gamma\gamma^T)\mathbf{F}^T$, both of which are trivially bounded under isotropy but require dedicated concentration arguments under anisotropy. The restriction $\beta < 1/2$ enters here to ensure these concentration bounds hold.

The main new difficulty, however, arises not in the universality statement itself but in *verifying its conditions*—showing that conditions (6) and (7) hold for the Hermite surrogate—which is the content of Theorem 2 and where the phase transition mechanism emerges (see the proof discussion therein). We provide the complete proof in Appendix A. \square

Theorem 1 is more general than a reduction to a single surrogate model: it establishes that *any* two activations with matched moment structure yield identical RFM performance under spiked data. We exploit this generality next by choosing $\hat{\sigma}$ to be a finite-degree Hermite polynomial, which makes the effective nonlinear structure of the RFM explicit.

4.2 EQUIVALENT NOISY POLYNOMIAL MODEL AND THE ROLE OF η

We now identify the surrogate that reveals the phase transition. The key tool is the Hermite expansion. For $i \in \mathbb{Z}^+$, the i -th Hermite polynomial is $H_i(x) := (-1)^i e^{x^2/2} \frac{d^i}{dx^i} e^{-x^2/2}$, and any activation σ with $\mathbb{E}_{z \sim \mathcal{N}(0,1)}[\sigma(z)^2] < \infty$ admits the expansion

$$\sigma(x) = \sum_{i=0}^{\infty} \frac{1}{i!} \mu_i H_i(x), \quad \text{with} \quad \mu_i := \mathbb{E}_{z \sim \mathcal{N}(0,1)} [H_i(z) \sigma(z)]. \quad (8)$$

The following theorem shows that, under spiked covariance, the RFM with activation σ is performance-equivalent to an RFM whose activation is a *finite-degree* Hermite polynomial plus noise. Crucially, the degree of this polynomial is governed by a single quantity η that encodes the interaction between input–label correlation, spike magnitude, and feature matrix.

Theorem 2. *Let σ be any activation function satisfying S.6. Define another activation function*

$$\hat{\sigma}_l(x) := \left(\sum_{j=0}^{l-1} \frac{1}{j!} \mu_j H_j(x) \right) + \mu_l^* z \quad \text{with} \quad z \sim \mathcal{N}(0,1), \quad (9)$$

where $\mu_j := \mathbb{E}_{z \sim \mathcal{N}(0,1)} [H_j(z) \sigma(z)]$ and $\mu_l^* := \sqrt{\mathbb{E}_{z \sim \mathcal{N}(0,1)} [\sigma(z)^2] - \sum_{j=0}^{l-1} \mu_j^2 / (j!)}$.

Suppose that assumptions S.1–S.6 given in Section 3 hold. If

$$\eta := \max_{1 \leq i \leq k} \left| \frac{(\boldsymbol{\xi} + \theta \alpha \boldsymbol{\gamma})^T \mathbf{f}_i}{\sqrt{1 + \theta \alpha^2}} \right| \leq \frac{C}{n^{1/l}}, \quad \text{for some } C > 0 \text{ and some } l \in \mathbb{Z}^+, \quad (10)$$

is satisfied, then

- (i) the training error \mathcal{T}_σ of the RFM with activation σ , and the training error $\mathcal{T}_{\hat{\sigma}_l}$ of the RFM with activation $\hat{\sigma}_l$, both converge in probability to the same value $e_\mathcal{T} \geq 0$,
- (ii) the corresponding generalization errors \mathcal{G}_σ and $\mathcal{G}_{\hat{\sigma}_l}$ also converge in probability to the same value $e_\mathcal{G} \geq 0$ under additional assumptions S.7 and S.8 provided in Appendix A.

Proof. We verify conditions (6) and (7) of Theorem 1 for the pair $(\sigma, \hat{\sigma}_l)$; the two equivalences require different arguments and interact differently with the spike.

Covariance equivalence. In Appendix C, we work with the transformed feature matrix $\hat{\mathbf{F}} := \mathbf{F}(\mathbf{I}_n + (\sqrt{1 + \theta} - 1)\boldsymbol{\gamma}\boldsymbol{\gamma}^T)$, whose rows no longer have uniform norms due to the spike. Via a Taylor expansion of $\mathbb{E}[\sigma(\hat{\mathbf{f}}_i^T \mathbf{g}) \sigma(\hat{\mathbf{f}}_j^T \mathbf{g})]$ with remainder bounds that absorb the spike-induced variance in $\|\hat{\mathbf{f}}_i\|^2$, we show

$$\left\| \mathbb{E}_{\mathbf{x}} [\sigma(\mathbf{F}\mathbf{x}) \sigma(\mathbf{F}\mathbf{x})^T] - (\mu_1^2 \mathbf{F}(\mathbf{I}_n + \theta \boldsymbol{\gamma}\boldsymbol{\gamma}^T) \mathbf{F}^T + \mu_*^2 \mathbf{I}_k) \right\| = \mathcal{O}(k^{-\varsigma}), \quad (11)$$

for some $\varsigma > 0$ and any σ satisfying S.6, with $\mu_1 = \mathbb{E}[z\sigma(z)]$ and $\mu_* = \sqrt{\mathbb{E}[\sigma(z)^2] - \mu_1^2}$ for $z \sim \mathcal{N}(0,1)$. Since $\hat{\sigma}_l$ preserves μ_1 and μ_* by construction, (11) holds for both σ and $\hat{\sigma}_l$ with the same right-hand side. The triangle inequality then gives

$$\left\| \mathbb{E}_{\mathbf{x}} [\sigma(\mathbf{F}\mathbf{x}) \sigma(\mathbf{F}\mathbf{x})^T] - \mathbb{E}_{\mathbf{x}} [\hat{\sigma}_l(\mathbf{F}\mathbf{x}) \hat{\sigma}_l(\mathbf{F}\mathbf{x})^T] \right\| = \mathcal{O}(k^{-\varsigma}). \quad (12)$$

Crucially, the covariance equivalence holds for *all* activations satisfying S.6, with no dependence on η ; the spike affects only the remainder bounds, not the structure of the result.

Cross-covariance equivalence. This is where the phase transition originates. In Appendix D, we decompose $\mathbb{E}[\sigma(\mathbf{f}_i^T \mathbf{x}) y]$ using the Hermite expansions of σ and σ_* . Under isotropy, each feature $\mathbf{f}_i^T \mathbf{x}$ and the label projection $\boldsymbol{\xi}^T \mathbf{x}$ are nearly independent—their correlation is $\mathcal{O}(n^{-1/2})$ —so only the first Hermite coefficient contributes, enforcing effective linearity. Under spiked covariance, the correlation $\eta_i = (\mathbf{f}_i^T \boldsymbol{\xi} + \theta \alpha \mathbf{f}_i^T \boldsymbol{\gamma}) / \sqrt{1 + \theta \alpha^2}$ can be substantially larger due to the $\theta \alpha$ amplification

term, and the Hermite decomposition retains contributions up to order l whenever $\eta^l \geq \tilde{C}n^{-1}$ for some $\tilde{C} > 0$. Bounding the remainder of this expansion under the condition $\eta = \mathcal{O}(n^{-1/l})$ yields

$$\left\| \mathbb{E}_{(\mathbf{x}, y)} [\sigma(\mathbf{F}\mathbf{x})y] - \mathbb{E}_{(\mathbf{x}, y)} [\hat{\sigma}_l(\mathbf{F}\mathbf{x})y] \right\| = \mathcal{O}(k^{-\varsigma}). \quad (13)$$

Applying Theorem 1 with (12) and (13) completes the proof. \square

Interpretation: η as the phase transition parameter Theorem 2 shows that the effective polynomial degree of the RFM is not intrinsic to the activation but is *selected by the data* through η . The quantity η is directly related to the input–label correlation: it depends on $(\boldsymbol{\xi} + \theta\alpha\boldsymbol{\gamma})/\sqrt{1 + \theta\alpha^2}$, which appears as the leading term in the decomposition

$$\mathbb{E}[(\mathbf{x} - \mathbb{E}[\mathbf{x}])(y - \mathbb{E}[y])] = \tilde{\mu}_1 \frac{\boldsymbol{\xi} + \theta\alpha\boldsymbol{\gamma}}{\sqrt{1 + \theta\alpha^2}} + \sum_{j>1} \tilde{\mu}_j \mathbb{E}_{\mathbf{x}}[\mathbf{x}H_j(\boldsymbol{\xi}^T \mathbf{x})], \quad (14)$$

where $\tilde{\mu}_j := \mathbb{E}_{z \sim \mathcal{N}(0,1)}[\sigma_*(z)H_j(z)]$. A larger value of $\|\boldsymbol{\xi} + \theta\alpha\boldsymbol{\gamma}\|/\sqrt{1 + \theta\alpha^2}$ implies a larger η for any \mathbf{F} sampled independently of $\boldsymbol{\gamma}$ and $\boldsymbol{\xi}$, and hence a higher effective polynomial degree. In particular, strong alignment (α large) combined with large spike magnitude (θ large) pushes η above the linear threshold, activating higher-order Hermite terms. This is the mechanism behind the phase transition.

4.3 THE LINEAR SIDE OF THE PHASE BOUNDARY

Setting $l = 2$ in Theorem 2 reduces the equivalent activation to $\hat{\sigma}_1(x) = \mu_0 + \mu_1 x + \mu_2^* z$, recovering the classical noisy linear surrogate (4). The following corollary gives the precise condition under which the RFM remains on the linear side of the phase boundary.

Corollary 3. *The noisy linear model (4) performs equivalent to the RFM with activation σ in terms of training and generalization errors if $\eta = \mathcal{O}(n^{-1/2})$ in (10).*

Remark 4. Corollary 3 provides a *sufficient* condition for effective linearity. The boundary $\eta = \mathcal{O}(n^{-1/2})$ in Figure 1a is therefore an upper bound on the linear regime: below it, the RFM is provably equivalent to the noisy linear model; above it, higher-order terms are *permitted* by the theory and are consistently observed in all our experiments (Figures 1–4).

Figure 1a displays the phase diagram. The red curve traces the boundary $\eta = \mathcal{O}(n^{-1/2})$ in the (α, θ) plane: below this curve, the RFM and the noisy linear model have indistinguishable generalization errors; above it, a gap opens and grows with α and θ . Since \mathbf{f}_i is sampled independently of $\boldsymbol{\gamma}$ and $\boldsymbol{\xi}$, both $|\boldsymbol{\gamma}^T \mathbf{f}_i|$ and $|\boldsymbol{\xi}^T \mathbf{f}_i|$ scale as $\mathcal{O}(n^{-1/2})$. The condition $\eta = \mathcal{O}(n^{-1/2})$ therefore reduces to $|\theta\alpha/\sqrt{1 + \theta\alpha^2}| = \mathcal{O}(1)$.

As a concrete example, consider the misaligned case $\alpha = \mathcal{O}(n^{-1/2})$, which arises with high probability when $\boldsymbol{\gamma}$ and $\boldsymbol{\xi}$ are drawn independently from $\mathcal{N}(0, \mathbf{I}_n)$ and normalized. Then $\eta = \mathcal{O}(n^{-1/2})$ holds for all $\theta \asymp n^\beta$ with $\beta \in [0, 1/2)$, placing the RFM firmly in the linear regime. Figure 1b confirms this: the generalization errors of the RFM and the noisy linear model coincide across activation functions.

4.4 THE NONLINEAR SIDE: HIGHER-ORDER POLYNOMIAL MODELS

When η exceeds the linear threshold of Corollary 3, the RFM crosses the phase boundary and the noisy linear surrogate no longer captures its performance. Theorem 2 provides the correct description on this side: the RFM is equivalent to the noisy polynomial model

$$\boldsymbol{\omega}^T \hat{\sigma}_l(\mathbf{F}\mathbf{x}), \quad (15)$$

for $l > 2$, where $\hat{\sigma}_l$ is defined in (9). The higher-order Hermite terms that were invisible in the linear regime now persist and actively reduce generalization error beyond what any linear predictor can achieve.

Which polynomial orders contribute depends not only on η but also on the interplay between the Hermite spectra of the activation σ and the teacher σ_* , as the following remark makes precise.

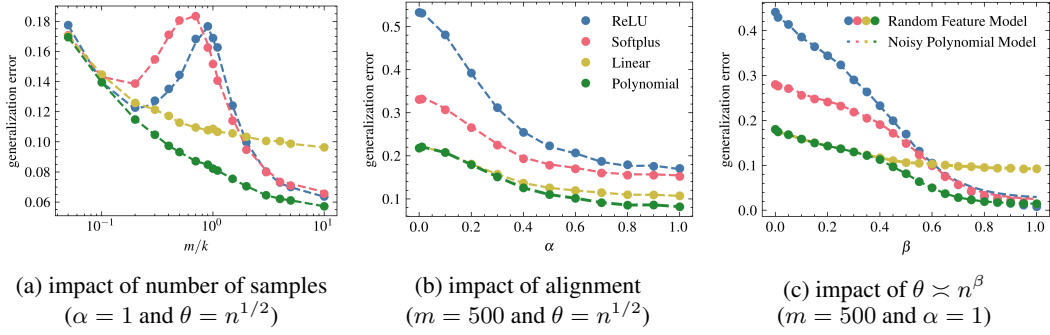


Figure 3: *Comparison of activation functions* - generalization errors of the RFM with different nonlinearities (linear, polynomial, Softplus, ReLU) with respect to number of samples (on the left), alignment (on the center), and spike magnitude $\theta \asymp n^\beta$ (on the right). Here, $n = 400$, $k = 500$, $\lambda = 10^{-2}$, and $\sigma_* = \sigma_{ReLU}$. We limit the degree of the equivalent polynomial model (9) to a maximum of $l = 4$ for numerical stability. We plot the average of 50 Monte Carlo runs.

Remark 5. When $\eta = \mathcal{O}(n^{-1/4})$, the equivalent activation is a third-degree polynomial. Let $\mu_0, \mu_1, \mu_2, \mu_3$ and $\tilde{\mu}_0, \tilde{\mu}_1, \tilde{\mu}_2, \tilde{\mu}_3$ denote the first four Hermite coefficients (8) of σ and σ_* , respectively. Then $\mathbb{E}[\hat{\sigma}_l(\mathbf{f}_i^T \mathbf{x})y] = \sum_{j=0}^3 \frac{1}{j!} \mu_j \tilde{\mu}_j \eta_j^j$ by (108). The polynomial model (15) therefore reduces to second degree if $\mu_3 \tilde{\mu}_3 = 0$, and collapses all the way to the noisy linear model (4) if additionally $\mu_2 \tilde{\mu}_2 = 0$. Thus, even above the phase boundary, the effective degree can be lower than the maximum permitted by η when the Hermite spectra of σ and σ_* are “mismatched” at certain orders.

Figure 2 illustrates Remark 5 in the aligned case ($\alpha = 1$, $\theta = n^{1/2}$), where the RFM is firmly on the nonlinear side of the phase boundary. In Figure 2a ($\sigma_* = \sigma_{ReLU}$), the noisy linear model suffices for tanh activation but not for ReLU, because tanh has $\mu_2 = 0$ while ReLU has $\mu_2 \neq 0$. Conversely, in Figure 2b ($\sigma_* = \sigma_{tanh}$), the situation reverses: tanh activation requires the polynomial surrogate ($\mu_3 \neq 0$) while ReLU does not ($\mu_3 = 0$). In both cases, the noisy polynomial model (15) accurately tracks the RFM. These results highlight that the effective degree on the nonlinear side of the phase boundary is jointly determined by the Hermite coefficients of σ and σ_* —the label-generation process is as important as the activation in determining which nonlinear terms contribute.

5 CROSSING THE PHASE BOUNDARY: NONLINEAR GAINS IN PRACTICE

The phase transition identified in Section 4 predicts that the RFM achieves genuinely nonlinear gains when the input–label correlation and spike magnitude push η above the linear threshold. We now verify this prediction numerically and quantify the gain across activation functions.

Baselines To isolate the effect of nonlinearity, we compare against two oracle baselines whose coefficients are tuned numerically to minimize generalization error. The first is an optimal linear activation,

$$\sigma_{linear}(x) = a_0 + a_1 x, \quad (16)$$

with $a_0, a_1 \in \mathbb{R}$. This represents the best possible performance achievable by any linear predictor in the RFM framework. The second is an optimal third-degree polynomial activation,

$$\sigma_{polynomial}(x) = b_0 + b_1 x + \frac{1}{2} b_2 (x^2 - 1) + \frac{1}{6} b_3 (x^3 - 3x) + b_4 z, \quad (17)$$

with $z \sim \mathcal{N}(0, 1)$ and $b_0, \dots, b_4 \in \mathbb{R}$ tuned analogously. This baseline captures the maximum performance permitted by Theorem 2 under $\eta = \mathcal{O}(n^{-1/4})$, which holds with high probability when $\beta < 1/2$.

Impact of sample size Figure 3a compares generalization errors as a function of m/k in the aligned case ($\alpha = 1$, $\theta = n^{1/2}$)—firmly on the nonlinear side of the phase boundary. The polynomial RFM consistently achieves the lowest generalization error across the full range of m/k ,

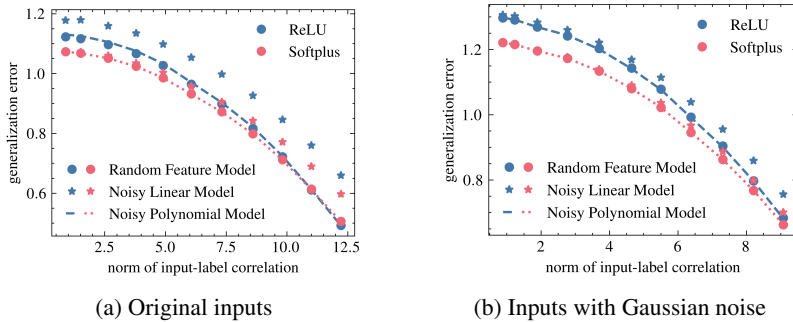


Figure 4: *The phase transition on real data: CIFAR-10 classification (airplane vs. automobile).* Input-label correlation is controlled by interpolating between true and random labels; the highest correlation norm uses true labels, the lowest uses random labels. As correlation increases, the RFM separates from the linear model, consistent with the predicted phase transition. Adding Gaussian noise (right) isolates the correlation effect. Here $l = 5$, $\lambda = 10^{-1}$, $k = n = 3072$, $m = 4000$; averages over 50 Monte Carlo runs. Details in Supplementary SM3.

confirming that higher-order terms provide a genuine advantage in this regime. ReLU and Softplus exhibit double descent Belkin et al. (2019); Geiger et al. (2020), causing the optimized linear activation to outperform them in the mid-range of m/k . However, the polynomial baseline avoids double descent entirely (its coefficients are optimized) and dominates throughout. These patterns are consistent with findings under isotropic data Wang & Bento (2022); Demir & Dogan (2024), but here the nonlinear gain itself is a consequence of being above the phase boundary.

Impact of alignment Figure 3b varies α while holding $\theta = n^{1/2}$ fixed, sweeping across the phase boundary. For $\alpha \leq 0.3$ the RFM is in the linear regime: the polynomial and linear baselines yield nearly identical errors, confirming that higher-order terms contribute negligibly. A gradual separation emerges for $0.3 < \alpha \leq 0.6$, and for $\alpha > 0.6$ the polynomial RFM distinctly outperforms the linear one. This progression directly traces the transition predicted by Theorem 2: as α increases, η grows, higher Hermite orders activate, and the nonlinear gain materializes.

Impact of spike magnitude Figure 3c varies the spike exponent β while holding $\alpha = 1$ fixed. Generalization errors for all activations decrease as the spike magnitude grows. For $\beta < 0.4$ the linear and polynomial baselines are indistinguishable— η remains near the linear threshold despite full alignment. As β increases past 0.4, the polynomial RFM separates from the linear one, confirming that the phase transition requires both sufficient alignment *and* sufficient spike magnitude. Notably, ReLU and Softplus continue to track their equivalent noisy polynomial models even beyond $\beta = 0.5$, suggesting the phase boundary extends beyond the range covered by our proofs.

6 REAL-WORLD VALIDATION

To test whether the predicted phase transition manifests beyond the spiked-covariance model, we study binary classification (airplane vs. automobile) on CIFAR-10 Krizhevsky et al. (2009). Figure 4a shows results on the original inputs. The noisy polynomial model tracks the RFM across all correlation levels, while the gap between the RFM and the noisy linear model grows with correlation strength—mirroring the phase transition on synthetic data. Furthermore, to isolate the role of input-label correlation from other structural properties of the covariance, we add standard Gaussian noise to the inputs so that the linear model matches the RFM at weak correlation. Figure 4b confirms that, even in this controlled setting, the generalization errors of the RFM and the linear model progressively separate as correlation increases. This demonstrates that the correlation-driven transition identified by our theory is not an artifact of the spiked model but reflects a mechanism that operates on real data. More broadly, many real-world datasets exhibit low intrinsic dimensionality Facco et al. (2017); Spigler et al. (2020), so that their covariance is well-approximated by a low-rank-plus-identity structure. Hence, the single-spike model captures the dominant mode of anisotropy, and the correlation between this mode and the label direction plays precisely the role of α in our theory.

7 CONCLUSION

We have identified a correlation-driven transition in the effective nonlinearity of random feature models under spiked covariance. The transition is governed by a single quantity η that couples input–label correlation, spike magnitude, and feature matrix: when $\eta = \mathcal{O}(n^{-1/2})$ the RFM is performance-equivalent to a noisy linear predictor; when η is larger, higher-order Hermite terms persist and the RFM achieves genuinely nonlinear gains. This characterization rests on two technical contributions—a universality theorem that extends beyond isotropic data, and an equivalent noisy polynomial surrogate whose effective degree is selected by the data through η —and is corroborated by numerical simulations and real-data experiments on CIFAR-10.

ACKNOWLEDGMENTS

This work is supported in part by the TÜBİTAK-ARDEB 1001 program under project 124E063. We extend our gratitude to TÜBİTAK for its support. S.D. is supported by an AI Fellowship provided by Koç University & İş Bank Artificial Intelligence (KUIS AI) Research Center and a PhD Scholarship (BİDEB 2211) from TÜBİTAK.

A PROOF OF UNIVERSALITY OF RANDOM FEATURES FOR THE SPIKED DATA

Here, we prove Theorem 1 by extending the Lindeberg replacement of Hu & Lu (2023) to the spiked covariance. For a given set of training samples $\{(\mathbf{x}_i, y_i)\}_{i=1}^m$, let $\mathbf{R} := [\mathbf{r}_1, \mathbf{r}_2, \dots, \mathbf{r}_m]^T$ where $\mathbf{r}_i := \sigma(\mathbf{F}\mathbf{x}_i)$ for all $i \in \{1, 2, \dots, m\}$. For a given \mathbf{R} , we introduce the following perturbed optimization:

$$\Phi_{\mathbf{R}}(\tau_1, \tau_2) := \inf_{\boldsymbol{\omega} \in \mathbb{R}^k} \left\{ \sum_{i=1}^m (\boldsymbol{\omega}^T \mathbf{r}_i - y_i)^2 + Q(\boldsymbol{\omega}) \right\}, \quad (18)$$

where $Q(\boldsymbol{\omega}) := m\lambda \|\boldsymbol{\omega}\|_2^2 + \tau_1 k \boldsymbol{\omega}^T \Sigma_x \boldsymbol{\omega} + \tau_2 k \boldsymbol{\omega}^T \Sigma_{xy}$ with $\Sigma_x := \mathbb{E}_{(\mathbf{x}, y)} [\sigma(\mathbf{F}\mathbf{x})\sigma(\mathbf{F}\mathbf{x})^T]$ and $\Sigma_{xy} := \mathbb{E}_{(\mathbf{x}, y)} [\sigma(\mathbf{F}\mathbf{x})y]$. Here, $Q(\boldsymbol{\omega})$ is a function of τ_1, τ_2 (in addition to $\boldsymbol{\omega}$) but we do not include them in the notation for simplicity. Note that $\Phi_{\mathbf{R}}(0, 0)/m$ is equal to the training error (\mathcal{T}_σ) of the original problem (2). The additional terms in $Q(\boldsymbol{\omega})$ are related to the generalization error and we discuss them later. Since we are interested in two different functions σ and $\hat{\sigma}$, we define $\mathbf{A} := [\mathbf{a}_1, \mathbf{a}_2, \dots, \mathbf{a}_m]^T$ and $\mathbf{B} := [\mathbf{b}_1, \mathbf{b}_2, \dots, \mathbf{b}_m]^T$ where $\mathbf{a}_i := \sigma(\mathbf{F}\mathbf{x}_i)$ and $\mathbf{b}_i := \hat{\sigma}(\mathbf{F}\mathbf{x}_i)$ for all $i \in \{1, 2, \dots, m\}$. Then, the training error \mathcal{T}_σ for the RFM with activation σ , and the training error $\mathcal{T}_{\hat{\sigma}}$ for the case of activation $\hat{\sigma}$ converge in probability to the same value $e_{\mathcal{T}} \geq 0$ if the following holds

$$\frac{\Phi_{\mathbf{A}}(0, 0)}{m} \xrightarrow{\mathbb{P}} e_{\mathcal{T}} \quad \text{and} \quad \frac{\Phi_{\mathbf{B}}(0, 0)}{m} \xrightarrow{\mathbb{P}} e_{\mathcal{T}}. \quad (19)$$

Since $\Phi_{\mathbf{R}}(0, 0)/m = (k/m)(\Phi_{\mathbf{R}}(0, 0)/k)$ and $(k/m) \in (0, \infty)$ by assumption S.4, we focus on $\Phi_{\mathbf{R}}(0, 0)/k$ for the rest of the proof in order to write the bounds in terms of k only.

Now, we describe how we handle the generalization error. We introduce $\tau_1 k \boldsymbol{\omega}^T \Sigma_x \boldsymbol{\omega} + \tau_2 k \boldsymbol{\omega}^T \Sigma_{xy}$ into $Q(\boldsymbol{\omega})$ to be used in the calculation of the generalization error. Before describing the relationship between the additional terms and the generalization error, we need the following two additional assumptions for the study of generalization error.

Additional Suppositions for Generalization Error

S.7 — There exists $\tau_* = \mathcal{O}(1/\sqrt{k})$ and $s \in (0, \infty)$ such that $Q(\boldsymbol{\omega})/m$ is s -strongly convex for all $\tau_1, \tau_2 \in (-\tau_*, \tau_*)$.

S.8 — There exists a limiting function $q^*(\tau_1, \tau_2)$ such that $\Phi_{\mathbf{R}}(\tau_1, \tau_2)/k \xrightarrow{\mathbb{P}} q^*(\tau_1, \tau_2)$ for all $\tau_1, \tau_2 \in (-\tau_*, \tau_*)$. Furthermore, the partial derivatives of $q^*(\tau_1, \tau_2)$ exist at $\tau_1 = \tau_2 = 0$, denoted as $\frac{\partial}{\partial \tau_1} q^*(0, 0) = \rho^*$ and $\frac{\partial}{\partial \tau_2} q^*(0, 0) = \pi^*$.

Assumption S.7 is required to keep the perturbed objective (18) convex and bound the norm of optimal ω of (18). Based on the assumption S.8, the generalization error of the RFM with σ can be specified as follows $\mathcal{G}_\sigma \xrightarrow{\mathbb{P}} \rho^* - 2\pi^* + \mathbb{E}_y[y^2]$. Furthermore, the generalization error \mathcal{G}_σ for the RFM with activation σ and the generalization error $\mathcal{G}_{\hat{\sigma}}$ for the case of activation $\hat{\sigma}$ converge in probability to the same value $e_G \geq 0$ if the following holds

$$\frac{\Phi_{\mathbf{A}}(\tau_1, \tau_2)}{k} \xrightarrow{\mathbb{P}} \phi \quad \text{and} \quad \frac{\Phi_{\mathbf{B}}(\tau_1, \tau_2)}{k} \xrightarrow{\mathbb{P}} \phi, \quad (20)$$

for any $\phi \in \mathbb{R}$ and any $\tau_1, \tau_2 \in (-\tau_*, \tau_*)$, a proof which is provided in Supplementary Lemma SM1. The rest of this appendix shows that (20) holds, which then implies the statement of Theorem 1. To show the convergence in probability (20), we take advantage of a test function $\varphi(x)$. Specifically, (20) holds if

$$\left| \mathbb{E} \varphi \left(\frac{1}{k} \Phi_{\mathbf{A}} \right) - \mathbb{E} \varphi \left(\frac{1}{k} \Phi_{\mathbf{B}} \right) \right| \leq \max \{ \|\varphi\|_\infty, \|\varphi'\|_\infty, \|\varphi''\|_\infty \} \kappa_k, \quad (21)$$

for some $\kappa_k = o(1)$ and every bounded test function $\varphi(x)$ which has bounded first two derivatives (for a proof, we refer to the Supplementary Lemma SM2). From now on, we use $\Phi_{\mathbf{R}}$ to denote $\Phi_{\mathbf{R}}(\tau_1, \tau_2)$. We can continue as follows

$$\begin{aligned} \left| \mathbb{E} \varphi \left(\frac{1}{k} \Phi_{\mathbf{A}} \right) - \mathbb{E} \varphi \left(\frac{1}{k} \Phi_{\mathbf{B}} \right) \right| &\leq \mathbb{E} \left| \mathbb{E}_{\setminus \mathbf{F}} \left[\varphi \left(\frac{1}{k} \Phi_{\mathbf{A}} \right) \right] - \mathbb{E}_{\setminus \mathbf{F}} \left[\varphi \left(\frac{1}{k} \Phi_{\mathbf{B}} \right) \right] \right|, \\ &= \mathbb{E} \left[\left| \mathbb{E}_{\setminus \mathbf{F}} \left[\varphi \left(\frac{1}{k} \Phi_{\mathbf{A}} \right) \right] - \mathbb{E}_{\setminus \mathbf{F}} \left[\varphi \left(\frac{1}{k} \Phi_{\mathbf{B}} \right) \right] \right| (\mathbb{1}_{\mathcal{A}}(\mathbf{F}) + \mathbb{1}_{\mathcal{A}^c}(\mathbf{F})) \right], \\ &\leq \sup_{\mathbf{F} \in \mathcal{A}} \left| \mathbb{E}_{\setminus \mathbf{F}} \left[\varphi \left(\frac{1}{k} \Phi_{\mathbf{A}} \right) \right] - \mathbb{E}_{\setminus \mathbf{F}} \left[\varphi \left(\frac{1}{k} \Phi_{\mathbf{B}} \right) \right] \right| + 2\|\varphi\|_\infty \mathbb{P}(\mathcal{A}^c), \end{aligned} \quad (22)$$

where $\mathbb{E}_{\setminus \mathbf{F}}[\cdot]$ denotes the conditional expectation for a fixed feature matrix \mathbf{F} and $\mathbb{1}_{\mathcal{A}}(\mathbf{F})$ is a indicator function (1 if $\mathbf{F} \in \mathcal{A}$). We refer to \mathcal{A} as the admissible set of feature matrices defined in Appendix B. We also have $\mathbb{P}(\mathcal{A}^c) = o(1)$, proof of which is also given in Appendix B. Now, we need to show

$$\sup_{\mathbf{F} \in \mathcal{A}} \left| \mathbb{E}_{\setminus \mathbf{F}} \varphi \left(\frac{1}{k} \Phi_{\mathbf{A}} \right) - \mathbb{E}_{\setminus \mathbf{F}} \varphi \left(\frac{1}{k} \Phi_{\mathbf{B}} \right) \right| \leq \max \{ \|\varphi'\|_\infty, \|\varphi''\|_\infty \} \kappa_k, \quad (23)$$

for some $\kappa_k = o(1)$. To find a useful bound for (23), we interpolate the path from $\Phi_{\mathbf{A}}$ to $\Phi_{\mathbf{B}}$ following Lindeberg's method Lindeberg (1922); Korada & Montanari (2011)

$$\Phi_t := \min_{\omega \in \mathbb{R}^k} \left\{ \sum_{i=1}^t (\omega^T \mathbf{b}_i - y_i)^2 + \sum_{i=t+1}^m (\omega^T \mathbf{a}_i - y_i)^2 + Q(\omega) \right\}, \quad (24)$$

$$\hat{\omega}_t := \arg \min_{\omega \in \mathbb{R}^k} \left\{ \sum_{i=1}^t (\omega^T \mathbf{b}_i - y_i)^2 + \sum_{i=t+1}^m (\omega^T \mathbf{a}_i - y_i)^2 + Q(\omega) \right\}, \quad (25)$$

for $0 \leq t \leq m$. Then,

$$\left| \mathbb{E}_{\setminus \mathbf{F}} \varphi \left(\frac{1}{k} \Phi_{\mathbf{A}} \right) - \mathbb{E}_{\setminus \mathbf{F}} \varphi \left(\frac{1}{k} \Phi_{\mathbf{B}} \right) \right| \leq \sum_{t=1}^m \left| \mathbb{E}_{\setminus \mathbf{F}} \varphi \left(\frac{1}{k} \Phi_t \right) - \mathbb{E}_{\setminus \mathbf{F}} \varphi \left(\frac{1}{k} \Phi_{t-1} \right) \right|, \quad (26)$$

due to triangle inequality. Therefore, we focus on showing the following

$$\left| \mathbb{E}_{\setminus \mathbf{F}} \varphi \left(\frac{1}{k} \Phi_t \right) - \mathbb{E}_{\setminus \mathbf{F}} \varphi \left(\frac{1}{k} \Phi_{t-1} \right) \right| \leq \max \{ \|\varphi'\|_\infty, \|\varphi''\|_\infty \} \frac{\kappa_k}{k}, \quad (27)$$

since $k/m \in (0, \infty)$. Here, Φ_t and Φ_{t-1} can be seen as perturbations of a common ‘‘leave-one-out’’ problem defined as

$$\Phi_{\setminus t} := \min_{\omega \in \mathbb{R}^k} \left\{ \sum_{i=1}^{t-1} (\omega^T \mathbf{b}_i - y_i)^2 + \sum_{i=t+1}^m (\omega^T \mathbf{a}_i - y_i)^2 + Q(\omega) \right\}, \quad (28)$$

$$\hat{\omega}_{\setminus t} := \arg \min_{\omega \in \mathbb{R}^k} \left\{ \sum_{i=1}^{t-1} (\omega^T \mathbf{b}_i - y_i)^2 + \sum_{i=t+1}^m (\omega^T \mathbf{a}_i - y_i)^2 + Q(\omega) \right\}. \quad (29)$$

Note that t -th sample is left out in the definition of $\Phi_{\setminus t}$ and $\omega_{\setminus t}$. Since $\Phi_t \approx \Phi_{\setminus t}$, we apply Taylor's expansion around $\Phi_{\setminus t}$

$$\varphi\left(\frac{1}{k}\Phi_t\right) = \varphi\left(\frac{1}{k}\Phi_{\setminus t}\right) + \frac{1}{k}\varphi'\left(\frac{1}{k}\Phi_{\setminus t}\right)(\Phi_t - \Phi_{\setminus t}) + \frac{1}{2k^2}\varphi''(\zeta)(\Phi_t - \Phi_{\setminus t})^2, \quad (30)$$

where ζ is some value that lies between $\frac{1}{k}\Phi_t$ and $\frac{1}{k}\Phi_{\setminus t}$. Similarly, applying Taylor's expansion to $\varphi(\Phi_{t-1})$ around $\Phi_{\setminus t}$, and then subtracting it from the last equation, we get

$$\begin{aligned} & \left| \mathbb{E}_{\mathbf{F}} \left[\varphi\left(\frac{1}{k}\Phi_t\right) \right] - \mathbb{E}_{\mathbf{F}} \left[\varphi\left(\frac{1}{k}\Phi_{t-1}\right) \right] \right| \\ & \leq \frac{\|\varphi'(x)\|_{\infty}}{k} \mathbb{E}_{\mathbf{F}} |\mathbb{E}_t(\Phi_t - \Phi_{t-1})| + \frac{\|\varphi''(x)\|_{\infty}}{2k} \frac{\left(\mathbb{E}_{\mathbf{F}}(\Phi_t - \Phi_{\setminus t})^2 + \mathbb{E}_{\mathbf{F}}(\Phi_{t-1} - \Phi_{\setminus t})^2 \right)}{k}, \end{aligned} \quad (31)$$

where \mathbb{E}_t denotes the conditional expectation over the random vectors $\{\mathbf{a}_t, \mathbf{b}_t\}$ associated with the t -th training sample, while $\{\mathbf{a}_i, \mathbf{b}_i\}_{i \neq t}$ and \mathbf{F} are fixed.

To bound the terms on the right side of (31), we first define a surrogate optimization problem:

$$\Psi_t(\mathbf{r}) := \Phi_{\setminus t} + \min_{\omega \in \mathbb{R}^k} \left\{ \frac{1}{2} (\omega - \hat{\omega}_{\setminus t})^T \mathbf{H}_{\setminus t} (\omega - \hat{\omega}_{\setminus t}) + (\omega^T \mathbf{r} - y_t)^2 \right\}, \quad (32)$$

where

$$\mathbf{H}_{\setminus t} := 2 \sum_{i=1}^{t-1} \mathbf{b}_i \mathbf{b}_i^T + 2 \sum_{i=t+1}^m \mathbf{a}_i \mathbf{a}_i^T + \nabla^2 Q(\hat{\omega}_{\setminus t}) \quad (33)$$

is the the Hessian matrix of the objective function $\Phi_{\setminus t}$ evaluated at $\hat{\omega}_{\setminus t}$. Next, we have the following Lemma proven in Supplementary Lemma SM3, which makes $\Psi_t(\mathbf{r})$ particularly interesting.

Lemma 6. $\Phi_{t-1} = \Psi_t(\mathbf{a}_t)$, and $\Phi_t = \Psi_t(\mathbf{b}_t)$ hold in this setting.

We continue by simplifying $\Psi_t(\mathbf{r})$ as follows:

$$\Psi_t(\mathbf{r}) := \Phi_{\setminus t} + \min_{\omega \in \mathbb{R}^k} \left\{ \frac{1}{2} (\omega - \hat{\omega}_{\setminus t})^T \mathbf{H}_{\setminus t} (\omega - \hat{\omega}_{\setminus t}) + (\omega^T \mathbf{r} - y_t)^2 \right\}, \quad (34)$$

$$= \Phi_{\setminus t} + \min_{\tau} \min_{\mathbf{r}^T (\omega - \hat{\omega}_{\setminus t}) = \tau} \left\{ \frac{1}{2} (\omega - \hat{\omega}_{\setminus t})^T \mathbf{H}_{\setminus t} (\omega - \hat{\omega}_{\setminus t}) + \left(\hat{\omega}_{\setminus t}^T \mathbf{r} + \tau - y_t \right)^2 \right\}, \quad (35)$$

$$= \Phi_{\setminus t} + \min_{\tau} \left\{ \frac{\tau^2}{2\nu_t(\mathbf{r})} + \left(\hat{\omega}_{\setminus t}^T \mathbf{r} + \tau - y_t \right)^2 \right\}, \quad \text{with } \nu_t(\mathbf{r}) := \mathbf{r}^T \mathbf{H}_{\setminus t}^{-1} \mathbf{r}, \quad (36)$$

$$= \Phi_{\setminus t} + \frac{\left(\hat{\omega}_{\setminus t}^T \mathbf{r} - y_t \right)^2}{2\nu_t(\mathbf{r}) + 1} \leq \Phi_{\setminus t} + \left(\hat{\omega}_{\setminus t}^T \mathbf{r} - y_t \right)^2, \quad (37)$$

where the inequality in the last line is achieved by using $\tau = 0$ in (36) while the rest of the steps are trivial. Next, as shown in Supplementary Lemma SM4, we have

$$\max \left\{ \mathbb{E}_{\mathbf{F}} (\Psi_t(\mathbf{b}_t) - \Phi_{\setminus t})^2, \mathbb{E}_{\mathbf{F}} (\Psi_t(\mathbf{a}_t) - \Phi_{\setminus t})^2 \right\} \leq k^{1-\epsilon} \text{polylog } k, \quad (38)$$

which holds uniformly over $\mathbf{F} \in \mathcal{A}$ and $t \in \{1, 2, \dots, m\}$ for some $\epsilon > 0$ satisfying $\theta^2 \leq n^{1-\epsilon}$. Then, we can reach

$$\frac{1}{k} \mathbb{E}_{\mathbf{F}} (\Phi_t - \Phi_{\setminus t})^2 = \frac{1}{k} \mathbb{E}_{\mathbf{F}} (\Psi_t(\mathbf{b}_t) - \Phi_{\setminus t})^2 = o(1), \quad (39)$$

and similarly,

$$\frac{1}{k} \mathbb{E}_{\mathbf{F}} (\Phi_{t-1} - \Phi_{\setminus t})^2 = \frac{1}{k} \mathbb{E}_{\mathbf{F}} (\Psi_t(\mathbf{a}_t) - \Phi_{\setminus t})^2 = o(1). \quad (40)$$

Next, by Lemma 6 and equation (36), we have

$$\mathbb{E}_{\setminus \mathbf{F}} |\mathbb{E}_k (\Phi_t - \Phi_{t-1})| = \mathbb{E}_{\setminus \mathbf{F}} |\mathbb{E}_t [\Psi_t(\mathbf{b}_t) - \Psi_t(\mathbf{a}_t)]|, \quad (41)$$

$$= \mathbb{E}_{\setminus \mathbf{F}} \left| \mathbb{E}_t \left[\frac{(\hat{\omega}_{\setminus t}^T \mathbf{b}_t - y_t)^2}{2\nu_t(\mathbf{b}_t) + 1} - \frac{(\hat{\omega}_{\setminus t}^T \mathbf{a}_t - y_t)^2}{2\nu_t(\mathbf{a}_t) + 1} \right] \right|, \quad (42)$$

$$\leq \frac{1}{2\bar{\nu}_t + 1} \mathbb{E}_{\setminus \mathbf{F}} \left| \mathbb{E}_t \left[(\hat{\omega}_{\setminus t}^T \mathbf{b}_t - y_t)^2 - (\hat{\omega}_{\setminus t}^T \mathbf{a}_t - y_t)^2 \right] \right| + \Delta_t(\mathbf{a}_t) + \Delta_t(\mathbf{b}_t), \quad (43)$$

where $\bar{\nu}_t := \mathbb{E}_t \nu_t(\mathbf{a}_t)$ and $\Delta_t(\mathbf{r})$ is defined as

$$\Delta_t(\mathbf{r}) := \mathbb{E}_{\setminus \mathbf{F}} \left| \mathbb{E}_t \left(\frac{1}{2\nu_t(\mathbf{r}) + 1} - \frac{1}{2\bar{\nu}_t + 1} \right) (\hat{\omega}_{\setminus t}^T \mathbf{r} - y_t)^2 \right|, \quad (44)$$

for which the following is expected to hold

$$\max \{ \Delta_t(\mathbf{a}_t), \Delta_t(\mathbf{b}_t) \} = o(1), \quad (45)$$

due to the concentration of $\nu_t(\mathbf{a}_t)$ and $\nu_t(\mathbf{b}_t)$ around $\bar{\nu}_t$ (Lemma 7) and the fact that $\frac{1}{2\bar{\nu}_t + 1} \leq C$ for some $C > 0$ by (37).

Lemma 7. *Suppose the definitions in Appendix A. Let $\epsilon > 0$ be a constant satisfying $\theta \leq n^{1/2 - \epsilon/2}$. For $\mathbf{r}_t = \mathbf{a}_t$ or $\mathbf{r}_t = \mathbf{b}_t$, we have*

$$\mathbb{P}(|\nu_t(\mathbf{r}_t) - \mathbb{E}_t[\nu_t(\mathbf{r}_t)]| > \delta) \leq ce^{-Ck^\epsilon \delta^2 / \text{polylog } k}, \quad (46)$$

for some $c, C > 0$. Furthermore,

$$\mathbb{E}_t[|\nu_t(\mathbf{r}_t) - \mathbb{E}_t[\nu_t(\mathbf{r}_t)]|^l] \leq 2c(l!)(Ck^\epsilon / \text{polylog } k)^{-l/2}, \quad (47)$$

for some $c, C > 0$ and any $l \in \mathbb{Z}^+$. Finally,

$$\left| \mathbb{E}_t \nu_t(\mathbf{a}_t) - \mathbb{E}_t \nu_t(\mathbf{b}_t) \right| = \mathcal{O}(k^{-\varsigma}), \quad (48)$$

for some $\varsigma > 0$.

Proof. Supplementary Lemma SM8 □

In bounding the remaining term, the following lemma (proven in Supplementary Lemma SM9) will be useful.

Lemma 8. *For any $l \in \mathbb{Z}^+$ and any $t \in \{0, \dots, m\}$, we have $\mathbb{E}_{\setminus \mathbf{F}} \|\hat{\omega}_t\|^l \leq \text{polylog } k$, and $\mathbb{E}_{\setminus \mathbf{F}} \|\hat{\omega}_{\setminus t}\|^l \leq \text{polylog } k$.*

Next, we bound the remaining term in (43) as

$$\mathbb{E}_{\setminus \mathbf{F}} \left| \mathbb{E}_t \left[(\hat{\omega}_{\setminus t}^T \mathbf{b}_t - y_t)^2 \right] - \mathbb{E}_t \left[(\hat{\omega}_{\setminus t}^T \mathbf{a}_t - y_t)^2 \right] \right|, \quad (49)$$

$$= \mathbb{E}_{\setminus \mathbf{F}} \left| \hat{\omega}_{\setminus t}^T \left(\mathbb{E}_t[\mathbf{b}_t \mathbf{b}_t^T] - \mathbb{E}_t[\mathbf{a}_t \mathbf{a}_t^T] \right) \hat{\omega}_{\setminus t} - 2\hat{\omega}_{\setminus t}^T \left(\mathbb{E}_t[\mathbf{b}_t y_t] - \mathbb{E}_t[\mathbf{a}_t y_t] \right) \right| \quad (50)$$

$$\stackrel{(a)}{\leq} \mathbb{E}_{\setminus \mathbf{F}} \left| \hat{\omega}_{\setminus t}^T \left(\mathbb{E}_t[\mathbf{b}_t \mathbf{b}_t^T] - \mathbb{E}_t[\mathbf{a}_t \mathbf{a}_t^T] \right) \hat{\omega}_{\setminus t} \right| + 2\mathbb{E}_{\setminus \mathbf{F}} \left| \hat{\omega}_{\setminus t}^T \left(\mathbb{E}_t[\mathbf{b}_t y_t] - \mathbb{E}_t[\mathbf{a}_t y_t] \right) \right| \quad (51)$$

$$\stackrel{(b)}{\leq} \mathbb{E}_{\setminus \mathbf{F}} \|\hat{\omega}_{\setminus t}\|^2 \mathbb{E}_{\setminus \mathbf{F}} \left\| \mathbb{E}_t[\mathbf{b}_t \mathbf{b}_t^T] - \mathbb{E}_t[\mathbf{a}_t \mathbf{a}_t^T] \right\| + 2\mathbb{E}_{\setminus \mathbf{F}} \|\hat{\omega}_{\setminus t}\| \mathbb{E}_{\setminus \mathbf{F}} \left\| \mathbb{E}_t[\mathbf{b}_t y_t] - \mathbb{E}_t[\mathbf{a}_t y_t] \right\| \quad (52)$$

$$\stackrel{(c)}{=} o(1), \quad (53)$$

where we use triangle inequality to reach (a). Then, we apply Cauchy-Schwarz inequality in order to reach (b). In the last step, we use a bound on $\mathbb{E}_{\setminus \mathbf{F}} \|\hat{\omega}_{\setminus t}\|^l$ (Lemma 8) with the equivalence of covariance matrices (6) and the equivalence of cross-covariance vectors (7) to reach (c). We can use (53) and (45) to bound the right-hand side of (43). Then, (39)-(43) together with (31) imply (27). Finally, (26)-(27) imply (23) and consequently (21), which completes our proof.

B ADMISSIBLE SET OF FEATURE MATRICES

A feature matrix $\mathbf{F} = [\mathbf{f}_1, \mathbf{f}_2, \dots, \mathbf{f}_k]^T$ is called admissible ($\mathbf{F} \in \mathcal{A}$) if it satisfies

$$\max_{1 \leq i, j \leq k} |\mathbf{f}_i^T \mathbf{f}_j + \theta \gamma^T \mathbf{f}_j \mathbf{f}_i^T \gamma - \delta_{ij}| \leq \frac{\text{polylog } k}{\sqrt{k}}, \quad (54)$$

$$\|\mathbf{F}(\mathbf{I}_n + (\sqrt{1 + \theta} - 1)\gamma\gamma^T)\| \leq \sqrt{\theta} \text{polylog } k, \quad (55)$$

where δ_{ij} denote the Kronecker delta. Note that (54) (see Lemma 9) and (55) (see Lemma 10) hold with high probability for $\mathbf{f}_i \sim \mathcal{N}\left(0, \frac{1}{n+\theta}\mathbf{I}_n\right)$ which is sampled independent of γ, ξ and \mathbf{f}_j for $i \neq j$.

Lemma 9. *Under assumptions S.1-S.6, the following holds with high probability*

$$\max_{1 \leq i < j \leq k} |\mathbf{f}_i^T \mathbf{f}_j + \theta \gamma^T \mathbf{f}_j \mathbf{f}_i^T \gamma| \leq \frac{\text{polylog } k}{\sqrt{k}}, \quad (56)$$

$$\max_{1 \leq i \leq k} \left| \|\mathbf{f}_i\|^2 + \theta(\gamma^T \mathbf{f}_i)^2 - 1 \right| \leq \frac{\text{polylog } k}{\sqrt{k}}. \quad (57)$$

Proof. We first apply triangle equality to reach

$$|\mathbf{f}_i^T \mathbf{f}_j + \theta \gamma^T \mathbf{f}_j \mathbf{f}_i^T \gamma| \leq |\mathbf{f}_i^T \mathbf{f}_j| + \theta |\gamma^T \mathbf{f}_j \mathbf{f}_i^T \gamma|, \quad (58)$$

$$\left| \|\mathbf{f}_i\|^2 + \theta(\gamma^T \mathbf{f}_i)^2 - 1 \right| \leq \left| \|\mathbf{f}_i\|^2 - \frac{n}{n+\theta} \right| + \theta \left| (\gamma^T \mathbf{f}_i)^2 - \frac{1}{n+\theta} \right|. \quad (59)$$

Next, we find probability bounds for each of the terms on the right-hand side of (58) and (59). Let's start with $|\mathbf{f}_i^T \mathbf{f}_j|$. Remember that $\mathbf{f}_i \sim \mathcal{N}\left(0, \frac{1}{n+\theta}\mathbf{I}_n\right)$. Then, for any $l \in \{1, \dots, n\}$, $f_{i,l}$ and $f_{j,l}$ are sub-Gaussian random variables with sub-Gaussian norm bounded by $\frac{C}{\sqrt{n+\theta}}$ for some $C > 0$ (Vershynin, 2018, Example 2.5.8). Therefore, $f_{i,l}f_{j,l}$ is a sub-exponential random variable with sub-exponential norm bounded by $\frac{C^2}{n+\theta}$ (Vershynin, 2018, Lemma 2.7.7). Since $\mathbf{f}_i^T \mathbf{f}_j = \sum_{l=1}^n f_{i,l}f_{j,l}$, we can apply Bernstein's inequality (Vershynin, 2018, Theorem 2.8.2)

$$\mathbb{P}\left(|\mathbf{f}_i^T \mathbf{f}_j| \geq \epsilon\right) \leq 2e^{-c \min\left(\frac{\epsilon^2}{K^2 n}, \frac{\epsilon}{K}\right)}, \quad (60)$$

where $K = C^2/(n+\theta)$ is the sub-exponential norm bound and $c > 0$ is a constant. We set $\epsilon = (\log k)^2/\sqrt{k}$ and apply union bound so that we get

$$\mathbb{P}\left(\max_{1 \leq i < j \leq k} |\mathbf{f}_i^T \mathbf{f}_j| \geq \frac{(\log k)^2}{\sqrt{k}}\right) \leq c_1 e^{-(\log k)^2/c_2}, \quad (61)$$

for some $c_1, c_2 > 0$. Note that we use $n/k \in (0, \infty)$ and $\theta \leq \sqrt{n}$ to write n and θ in terms of k . Also, we may reach the following inequality using the analogous steps:

$$\mathbb{P}\left(\max_{1 \leq i \leq k} \left| \|\mathbf{f}_i\|^2 - \frac{n}{n+\theta} \right| \geq \frac{(\log k)^2}{\sqrt{k}}\right) \leq c_1 e^{-(\log k)^2/c_2}, \quad (62)$$

for some $c_1, c_2 > 0$. Note that $n/(n+\theta)$ appears in the equation since $\mathbb{E}[\|\mathbf{f}_i\|^2] = n/(n+\theta)$. Now, we focus on $|\gamma^T \mathbf{f}_j \mathbf{f}_i^T \gamma|$. First, note that $(\mathbf{f}_i^T \gamma) \sim \mathcal{N}(0, 1/(n+\theta))$ since γ is a deterministic vector with $\|\gamma\| = 1$. Therefore, $(\mathbf{f}_i^T \gamma)$ and $(\mathbf{f}_j^T \gamma)$ are sub-Gaussian random variables with sub-Gaussian norm bounded by $\frac{C}{\sqrt{n+\theta}}$ for some $C > 0$ (Vershynin, 2018, Example 2.5.8) so $(\gamma^T \mathbf{f}_j \mathbf{f}_i^T \gamma)$ is a sub-exponential random variable with sub-exponential norm bounded by $\frac{C^2}{n+\theta}$ (Vershynin, 2018, Lemma 2.7.7). Thus, we have sub-exponential tail bound (Vershynin, 2018, Proposition 2.7.1) as follows

$$\mathbb{P}\left(|\gamma^T \mathbf{f}_j \mathbf{f}_i^T \gamma| \geq \epsilon\right) \leq 2e^{-C\epsilon(n+\theta)}, \quad (63)$$

for some $C > 0$. Setting $\epsilon = (\log k)^2/k$, we reach

$$\mathbb{P}\left(\max_{1 \leq i < j \leq k} |\gamma^T \mathbf{f}_j \mathbf{f}_i^T \gamma| \geq \frac{(\log k)^2}{k}\right) \leq 2e^{-C(\log k)^2}, \quad (64)$$

for some $C > 0$. Following the analogous steps, we also get

$$\mathbb{P}\left(\max_{1 \leq i \leq k} \left| (\mathbf{f}_i^T \boldsymbol{\gamma})^2 - \frac{1}{n + \theta} \right| \geq \frac{(\log k)^2}{k} \right) \leq 2e^{-C(\log k)^2}, \quad (65)$$

for some $C > 0$ since $\mathbb{E}[(\mathbf{f}_i^T \boldsymbol{\gamma})^2] = 1/(n + \theta)$. Using the found probability bounds for each of the terms on the right-hand side of (58) and (59), we complete the proof. \square

Lemma 10. *Under assumptions S.1-S.6, the following hold with high probability*

$$\|\mathbf{F}(\mathbf{I}_n + \theta \boldsymbol{\gamma} \boldsymbol{\gamma}^T) \mathbf{F}^T\| \leq \theta \text{polylog } k. \quad (66)$$

Proof. Using the triangle inequality, we get

$$\|\mathbf{F}(\mathbf{I}_n + \theta \boldsymbol{\gamma} \boldsymbol{\gamma}^T) \mathbf{F}^T\| \leq \|\mathbf{F} \mathbf{F}^T\| + \theta \|\mathbf{F} \boldsymbol{\gamma} \boldsymbol{\gamma}^T \mathbf{F}^T\|. \quad (67)$$

First, we focus on $\|\mathbf{F} \mathbf{F}^T\| = \|\mathbf{F}\|^2$. Here, we can take advantage of a well-known result on the spectral norm of Gaussian random matrices (Vershynin, 2018, Corollary 7.3.3):

$$\mathbb{P}\left(\|\mathbf{F}\| \geq \sqrt{\frac{n}{n + \theta}} + \sqrt{\frac{k}{n + \theta}} + \epsilon\right) \leq 2e^{-c(n + \theta)\epsilon^2}, \quad (68)$$

$$\mathbb{P}\left(\|\mathbf{F}\| \geq \sqrt{\frac{n}{n + \theta}} + 2\sqrt{\frac{k}{n + \theta}}\right) \leq 2e^{-ck} \quad (69)$$

for any $\epsilon > 0$ and some $c > 0$. This result indicates $\|\mathbf{F} \mathbf{F}^T\| \leq \text{polylog } k$ with high probability. Next, we work on $\|\mathbf{F} \boldsymbol{\gamma} \boldsymbol{\gamma}^T \mathbf{F}^T\|$. Since $(\mathbf{F} \boldsymbol{\gamma} \boldsymbol{\gamma}^T \mathbf{F}^T)_{i,j} = \mathbf{f}_i^T \boldsymbol{\gamma} \boldsymbol{\gamma}^T \mathbf{f}_j$, we may use the related results (64) - (65) from the proof of Lemma 9. Specifically, we have the following inequality with high probability

$$\max_{1 \leq i, j \leq k} \left| \boldsymbol{\gamma}^T \mathbf{f}_j \mathbf{f}_i^T \boldsymbol{\gamma} - \frac{\delta_{ij}}{n + \theta} \right| \leq \frac{\text{polylog } k}{k}, \quad (70)$$

$$\max_{1 \leq i, j \leq k} |\boldsymbol{\gamma}^T \mathbf{f}_j \mathbf{f}_i^T \boldsymbol{\gamma}| \leq \frac{\text{polylog } k}{k}, \quad (71)$$

where δ_{ij} denote the Kronecker delta function and we use $1/(n + \theta) < C/k$ for some $C > 0$ in reaching the last line. It follows that the following holds with high probability

$$\|\mathbf{F} \boldsymbol{\gamma} \boldsymbol{\gamma}^T \mathbf{F}^T\| \leq \|\mathbf{F} \boldsymbol{\gamma} \boldsymbol{\gamma}^T \mathbf{F}^T\|_F = \sqrt{\sum_{i=1}^k \sum_{j=1}^k (\mathbf{f}_i^T \boldsymbol{\gamma} \boldsymbol{\gamma}^T \mathbf{f}_j)^2} \leq \text{polylog } k. \quad (72)$$

Using (67), we combine the results and reach the statement of the lemma. \square

C EQUIVALENCE OF COVARIANCE MATRICES

Here, we show that (6) holds for any activation function σ satisfying assumption S.6 and a second activation function defined as $\hat{\sigma}(x) := \mu_1 x + \mu_* z$ where $z \sim \mathcal{N}(0, 1)$. Note that trivially we have $\mathbb{E}_{\mathbf{x}}[\hat{\sigma}(\mathbf{F}\mathbf{x})\hat{\sigma}(\mathbf{F}\mathbf{x})^T] = \mu_1^2 \mathbf{F}(\mathbf{I}_n + \theta \boldsymbol{\gamma} \boldsymbol{\gamma}^T \mathbf{F}^T) + \mu_*^2 \mathbf{I}_k$. The following lemma shows the equivalence of covariance matrices for the activation functions σ and $\hat{\sigma}$.

Lemma 11. *Under assumptions S.1-S.6 given in Section 3, the following holds*

$$\left\| \mathbb{E}_{\mathbf{x}}[\sigma(\mathbf{F}\mathbf{x})\sigma(\mathbf{F}\mathbf{x})^T] - (\mu_1^2 \hat{\mathbf{F}} \hat{\mathbf{F}}^T + \mu_*^2 \mathbf{I}_k) \right\| = \mathcal{O}(k^{-\varsigma}), \quad (73)$$

for some $\varsigma > 0$, where $\hat{\mathbf{F}} := \mathbf{F}(\mathbf{I}_n + (\sqrt{1 + \theta} - 1)\boldsymbol{\gamma} \boldsymbol{\gamma}^T)$.

Proof. (Hu & Lu, 2023, Lemma 5) showed $\|\mathbb{E}_{\mathbf{g}}[\sigma(\mathbf{F}\mathbf{g})\sigma(\mathbf{F}\mathbf{g})^T] - (\mu_1^2 \mathbf{F} \mathbf{F}^T + \mu_*^2 \mathbf{I}_k)\| = \mathcal{O}(k^{-\varsigma})$ for some $\varsigma > 0$ under $\mathbf{g} \sim \mathcal{N}(0, \mathbf{I}_n)$ and some other assumptions on \mathbf{F} matrix and activation function σ . Here, we adapt their proof to our case. First, note that we can consider $\sigma(\hat{\mathbf{F}}\mathbf{g})$

instead of $\sigma(\mathbf{F}\mathbf{x})$ since $\sigma(\hat{\mathbf{F}}\mathbf{g})$ is equal (in distribution) to $\sigma(\mathbf{F}\mathbf{x})$. Now, our goal is to show $\|\mathbb{E}_{\mathbf{g}}[\sigma(\hat{\mathbf{F}}\mathbf{g})\sigma(\hat{\mathbf{F}}\mathbf{g})^T] - (\mu_1^2\hat{\mathbf{F}}\hat{\mathbf{F}}^T + \mu_*^2\mathbf{I}_k)\| = \mathcal{O}(k^{-\varsigma})$ for some $\varsigma > 0$. The (i, j) -th entry of $\mathbb{E}_{\mathbf{g}}[\sigma(\hat{\mathbf{F}}\mathbf{g})\sigma(\hat{\mathbf{F}}\mathbf{x})^T]$ is $\mathbb{E}\left[\sigma\left(\hat{\mathbf{f}}_i^T\mathbf{g}\right)\sigma\left(\hat{\mathbf{f}}_j^T\mathbf{g}\right)\right]$. Since $(\hat{\mathbf{f}}_i^T\mathbf{g}, \hat{\mathbf{f}}_j^T\mathbf{g})$ are jointly Gaussian, we can rewrite their joint distribution as that of $(z_i, \rho_{ij}z_i + \sqrt{1 - \rho_{ij}\rho_{ji}}z_j)$, where $z_i \sim \mathcal{N}(0, \|\hat{\mathbf{f}}_i\|^2)$, $z_j \sim \mathcal{N}(0, \|\hat{\mathbf{f}}_j\|^2)$ are two independent Gaussian variables and $\rho_{ij} := \hat{\mathbf{f}}_i^T\hat{\mathbf{f}}_j/\|\hat{\mathbf{f}}_i\|\|\hat{\mathbf{f}}_j\|$. Then, for $i \neq j$, we have,

$$\mathbb{E}\left[\sigma\left(\hat{\mathbf{f}}_i^T\mathbf{g}\right)\sigma\left(\hat{\mathbf{f}}_j^T\mathbf{g}\right)\right] = \mathbb{E}\left[\sigma\left(z_i\right)\sigma\left(\rho_{ij}z_i + \sqrt{1 - \rho_{ij}\rho_{ji}}z_j\right)\right], \quad (74)$$

$$\stackrel{(a)}{=} \mathbb{E}\left[\sigma\left(z_i\right)\sigma\left(\sqrt{1 - \rho_{ij}\rho_{ji}}z_j\right)\right] + \rho_{ij}\mathbb{E}\left[\sigma\left(z_i\right)z_i\sigma'\left(\sqrt{1 - \rho_{ij}\rho_{ji}}z_j\right)\right] \\ + \frac{1}{2}\rho_{ij}^2\mathbb{E}\left[\sigma\left(z_i\right)z_i^2\sigma''\left(\sqrt{1 - \rho_{ij}\rho_{ji}}z_j\right)\right] + \frac{1}{6}\rho_{ij}^3\mathbb{E}\left[\sigma\left(z_i\right)z_i^3\sigma'''\left(\zeta_{ij}\right)\right], \quad (75)$$

$$\stackrel{(b)}{=} \hat{\mathbf{f}}_i^T\hat{\mathbf{f}}_j\mathbb{E}\sigma'\left(z_i\right)\mathbb{E}\sigma'\left(\sqrt{1 - \rho_{ij}\rho_{ji}}z_j\right) + \frac{1}{6}\rho_{ij}^3\mathbb{E}\left[\sigma\left(z_i\right)z_i^3\sigma'''\left(\zeta_{ij}\right)\right], \quad (76)$$

$$\stackrel{(c)}{=} \hat{\mathbf{f}}_i^T\hat{\mathbf{f}}_j\mathbb{E}\sigma'\left(z_i\right)\mathbb{E}\sigma'\left(z_j\right) + R_{ij}, \quad (77)$$

where ζ_{ij} is some point between $\sqrt{1 - \rho_{ij}\rho_{ji}}z_j$ and $\rho_{ij}z_i + \sqrt{1 - \rho_{ij}\rho_{ji}}z_j$. Here, we apply Taylor's series expansion of $\sigma(\rho_{ij}z_i + \sqrt{1 - \rho_{ij}\rho_{ji}}z_j)$ around $\sqrt{1 - \rho_{ij}\rho_{ji}}z_j$ to reach (a). Then, we use the independence between z_i and z_j , and the following identities: $\mathbb{E}\sigma(z_i) = \mathbb{E}[\sigma(z_i)z_i^2] = 0$ (due to σ being an odd function) and $\mathbb{E}[\sigma(z_i)z_i] = \|\hat{\mathbf{f}}_i\|^2\mathbb{E}[\sigma'(z_i)]$ (by Stein's lemma). To reach (c), we define the remainder term R_{ij} as

$$R_{ij} = \hat{\mathbf{f}}_i^T\hat{\mathbf{f}}_j\mathbb{E}\sigma'\left(z_i\right)\left(\mathbb{E}\sigma'\left(\sqrt{1 - \rho_{ij}\rho_{ji}}z_j\right) - \mathbb{E}\sigma'\left(z_j\right)\right) + \frac{1}{6}\rho_{ij}^3\mathbb{E}\left[\sigma\left(z_i\right)z_i^3\sigma'''\left(\zeta_{ij}\right)\right]. \quad (78)$$

For $i = j$, we define $R_{ii} = 0$. Then, we can verify the following decomposition using (77):

$$\mathbb{E}[\sigma(\hat{\mathbf{F}}\mathbf{g})\sigma(\hat{\mathbf{F}}\mathbf{g})^T] = (\mu_1\mathbf{I}_k + \mathbf{D}_1)\hat{\mathbf{F}}\hat{\mathbf{F}}^T(\mu_1\mathbf{I}_k + \mathbf{D}_1) + \mu_*^2\mathbf{I}_k + \mathbf{D}_2 + \mathbf{D}_3 + \mathbf{R} \quad (79)$$

where we define $\mathbf{D}_1, \mathbf{D}_2, \mathbf{D}_3$ to be diagonal matrices as follows: $\mathbf{D}_1 := \text{diag}(\mathbb{E}\sigma'(z_i) - \mu_1)$, $\mathbf{D}_2 = \text{diag}(\mu_1^2 - \|\hat{\mathbf{f}}_i\|^2(\mathbb{E}\sigma'(z_i))^2)$, and $\mathbf{D}_3 = \text{diag}(\mathbb{E}\sigma^2(z_i) - \mu_1^2 - \mu_*^2)$.

Then, we have

$$\left\|\mathbb{E}[\sigma(\mathbf{F}\mathbf{x})\sigma(\mathbf{F}\mathbf{x})^T] - (\mu_1^2\hat{\mathbf{F}}\hat{\mathbf{F}}^T + \mu_*^2\mathbf{I}_k)\right\| \leq (2\mu_1 + \|\mathbf{D}_1\|)\|\hat{\mathbf{F}}\|^2\|\mathbf{D}_1\| + \|\mathbf{D}_2\| + \|\mathbf{D}_3\| + \|\mathbf{R}\|, \quad (80)$$

$$\leq \frac{\|\hat{\mathbf{F}}\|^2 \text{polylog } k}{\sqrt{k}} = \mathcal{O}(k^{-\varsigma}), \quad (81)$$

for some $\varsigma > 0$, where Lemma 12 is used for the bounds of $\|\mathbf{D}_1\|, \|\mathbf{D}_2\|, \|\mathbf{D}_3\|$ and $\|\mathbf{R}\|$. To reach the conclusion, we then take advantage of $\|\hat{\mathbf{F}}\|^2 \leq k^{1/2-\epsilon/2} \text{polylog } k$ (for some $\epsilon > 0$ satisfying $\theta \leq n^{1/2-\epsilon/2}$), which is due to (55). \square

The following lemmas are auxiliary results used in the proof of the lemma above.

Lemma 12. *Suppose the setting in Lemma 11 and the definitions in its proof. Then,*

$$\max\{\|\mathbf{D}_1\|, \|\mathbf{D}_2\|, \|\mathbf{D}_3\|, \|\mathbf{R}\|\} \leq \frac{\text{polylog } k}{\sqrt{k}}. \quad (82)$$

Proof. Before bounding the terms, we define a truncated version of the activation function σ as

$$\sigma_\epsilon(x) := \begin{cases} \sigma(x), & \text{if } |x| < \epsilon, \\ 0, & \text{otherwise,} \end{cases} \quad (83)$$

for $\epsilon = 2\log k$, which is useful due to Lemma 13. Furthermore, $\sigma_\epsilon(x)$, its finite powers and its derivatives are bounded due to assumption S.6. First, we focus on \mathbf{D}_1

$$\|\mathbf{D}_1\| \leq \max_i \mathbb{E}|\sigma'(z_i) - \mu_1| \quad (84)$$

$$\leq \max_i \mathbb{E}_{z \sim \mathcal{N}(0,1)} |\sigma'(\|\hat{\mathbf{f}}_i\|z) - \sigma'(z)| \quad (85)$$

$$\leq \max_i \mathbb{E}_{z \sim \mathcal{N}(0,1)} |\sigma'_\epsilon(\|\hat{\mathbf{f}}_i\|z) - \sigma'_\epsilon(z)| + \frac{\text{polylog } k}{k^{\log k}} \quad (86)$$

$$\leq (\|\sigma''_\epsilon(x)\|_\infty \mathbb{E}[|z|]) \max_i \left| \|\hat{\mathbf{f}}_i\| - 1 \right| + \frac{\text{polylog } k}{k^{\log k}} \quad (87)$$

$$\leq (\|\sigma''_\epsilon(x)\|_\infty \mathbb{E}[|z|]) \max_i \left| \|\hat{\mathbf{f}}_i\|^2 - 1 \right| + \frac{\text{polylog } k}{k^{\log k}} \leq \frac{\text{polylog } k}{\sqrt{k}}, \quad (88)$$

where we use Lemma 13 to get (86) and while the last line is due to (54) (Lemma 9) and bounded second derivative of σ_ϵ . Similarly, one can show $\|\mathbf{D}_2\| \leq \text{polylog } k/\sqrt{k}$. Next, we study $\|\mathbf{D}_3\|$ as

$$\|\mathbf{D}_3\| \leq \max_i |\mathbb{E}\sigma^2(z_i) - \mu_1^2 - \mu_*^2| \quad (89)$$

$$= \max_i \mathbb{E}_{z \sim \mathcal{N}(0,1)} |\sigma^2(\|\hat{\mathbf{f}}_i\|z) - \sigma^2(z)| \quad (90)$$

$$= \max_i \mathbb{E}_{z \sim \mathcal{N}(0,1)} |\sigma^2_\epsilon(\|\hat{\mathbf{f}}_i\|z) - \sigma^2_\epsilon(z)| + \frac{\text{polylog } k}{k^{\log k}} \quad (91)$$

$$\leq \text{polylog } k \max_i \left| \|\hat{\mathbf{f}}_i\| - 1 \right| + \frac{\text{polylog } k}{k^{\log k}} \quad (92)$$

$$\leq \text{polylog } k \max_i \left| \|\hat{\mathbf{f}}_i\|^2 - 1 \right| + \frac{\text{polylog } k}{k^{\log k}} \leq \frac{\text{polylog } k}{\sqrt{k}}, \quad (93)$$

where we use the bounded derivative of σ_ϵ^2 to reach (92) while the rest is similar to the bounding of $\|\mathbf{D}_1\|$. Lastly, to bound $\|\mathbf{R}\|$, one can first easily show that

$$\max_{1 \leq i, j \leq k} |R_{ij}| \leq \frac{\text{polylog } k}{k\sqrt{k}}. \quad (94)$$

using (54) (Lemma 9) and the definition of R_{ij} in (78). Then, we have

$$\|\mathbf{R}\| \leq \|\mathbf{R}\|_F = \left(\sum_{i=1}^k \sum_{j=1}^k R_{ij}^2 \right)^{1/2} \leq \frac{\text{polylog } k}{\sqrt{k}}, \quad (95)$$

which concludes our proof. \square

Lemma 13. *Let $f : \mathbb{R} \rightarrow \mathbb{R}$ be a function satisfying $|f(x)| \leq C(1 + |x|^K)$ for all $x \in \mathbb{R}$ and some constants $C > 0, K \in \mathbb{Z}^+$. Furthermore, define a truncated version of f as*

$$f_\epsilon(x) := \begin{cases} f(x), & \text{if } |x| < \epsilon, \\ 0, & \text{otherwise,} \end{cases} \quad (96)$$

for $\epsilon > 0$. If $\epsilon = 2\log k$, the following holds for any constant $a > 0$ and $z \sim \mathcal{N}(0, 1)$,

$$\mathbb{E}_z |f(az) - f_\epsilon(az)| = \frac{\text{polylog } k}{k^{\log k}}. \quad (97)$$

Proof. Supplementary Lemma SM10 \square

D EQUIVALENCE OF CROSS-COVARIANCE VECTORS

Here, we are interested in the cross-covariance $\mathbb{E}[\sigma(\mathbf{F}\mathbf{x})y]$.

In showing the equivalence of the cross-covariance vectors, we use the following lemma describing the orthogonality of Hermite polynomials.

Lemma 14. Let $H_i(x)$ be the probabilist's i -th Hermite polynomial and $z_1, z_2 \stackrel{i.i.d.}{\sim} \mathcal{N}(0, 1)$. Then, for any $\rho \in [0, 1]$ and any $c \geq |\rho|$,

$$\mathbb{E}_{z_1, z_2} [H_i(\rho z_1 + \sqrt{c^2 - \rho^2} z_2) H_j(z_1)] = (i!) \rho^i \delta_{i,j}, \quad (98)$$

where δ_{ij} is Kronecker delta function.

Proof. Supplementary Lemma SM11 □

The following lemma specifies the equivalence of the cross-covariance vectors for the activation function σ and its finite-degree Hermite expansion $\hat{\sigma}_l$.

Lemma 15. Suppose assumptions S.1-S.6. Let $\eta_i := \mathbb{E} \left[\frac{(\mathbf{f}_i \mathbf{x})(\boldsymbol{\xi}^T \mathbf{x})}{\sqrt{1+\theta\alpha^2}} \right] = \frac{\mathbf{f}_i^T \boldsymbol{\xi} + \theta \alpha \mathbf{f}_i^T \boldsymbol{\gamma}}{\sqrt{1+\theta\alpha^2}}$. Assume that

$$\eta := \max_{1 \leq i \leq k} |\eta_i| \leq \frac{C}{n^{1/l}}, \quad \text{for some } C > 0 \text{ and some } l \in \mathbb{Z}^+. \quad (99)$$

Then, the following holds

$$\left\| \mathbb{E}_{(\mathbf{x}, y)} [\sigma(\mathbf{F}\mathbf{x})y] - \mathbb{E}_{(\mathbf{x}, y)} [\hat{\sigma}_l(\mathbf{F}\mathbf{x})y] \right\| = \mathcal{O}(k^{-\varsigma}), \quad (100)$$

for some $\varsigma > 0$ and $\hat{\sigma}_l(x)$ defined in (9).

Proof. Let $\mathbf{x} \sim \mathcal{N}(0, \mathbf{I}_k + \theta \boldsymbol{\gamma} \boldsymbol{\gamma}^T)$. By assumption S.3, we have

$$\mathbb{E}_{(\mathbf{x}, y)} [\sigma(\mathbf{F}\mathbf{x})y] = \mathbb{E}_{\mathbf{x}} \left[\sigma(\mathbf{F}\mathbf{x}) \sigma_* \left(\frac{\boldsymbol{\xi}^T \mathbf{x}}{\sqrt{1+\theta\alpha^2}} \right) \right] = \mathbb{E}_{\mathbf{g}} \left[\sigma(\hat{\mathbf{F}}\mathbf{g}) \sigma_* \left(\hat{\boldsymbol{\xi}}^T \mathbf{g} \right) \right], \quad (101)$$

where $\mathbf{g} \sim \mathcal{N}(0, \mathbf{I}_n)$, $\hat{\mathbf{F}} := \mathbf{F}(\mathbf{I}_n + (\sqrt{1+\theta} - 1)\boldsymbol{\gamma} \boldsymbol{\gamma}^T)$ and $\hat{\boldsymbol{\xi}} := \frac{(\mathbf{I}_n + (\sqrt{1+\theta} - 1)\boldsymbol{\gamma} \boldsymbol{\gamma}^T) \boldsymbol{\xi}}{\sqrt{1+\theta\alpha^2}}$. Before dealing with the functions σ and σ_* , we consider the joint distribution of $(\hat{\mathbf{f}}_i^T \mathbf{g}, \hat{\boldsymbol{\xi}}^T \mathbf{g})$, which is jointly Gaussian

$$(\hat{\mathbf{f}}_i^T \mathbf{g}, \hat{\boldsymbol{\xi}}^T \mathbf{g}) \sim \mathcal{N} \left(0, \begin{bmatrix} \|\hat{\mathbf{f}}_i\|^2 & \eta_i \\ \eta_i & 1 \end{bmatrix} \right), \quad (102)$$

Indeed, we can write an equivalent of $(\hat{\mathbf{f}}_i^T \mathbf{g}, \hat{\boldsymbol{\xi}}^T \mathbf{g})$ as $(\eta_i z + \sqrt{\|\hat{\mathbf{f}}_i\|^2 - \eta_i^2} z_i, z)$, where $z_i, z \stackrel{i.i.d.}{\sim} \mathcal{N}(0, 1)$. This decomposition will be useful since we split correlated part $\eta_i z$ and uncorrelated part $\sqrt{\|\hat{\mathbf{f}}_i\|^2 - \eta_i^2} z_i$. Now, we use Hermite expansions of σ and σ_*

$$\sigma(x) = \sum_{j=0}^{\infty} \frac{1}{j!} \mu_j H_j(x), \quad \text{and} \quad \sigma_*(x) = \sum_{j=0}^{\infty} \frac{1}{j!} \tilde{\mu}_j H_j(x), \quad (103)$$

where $H_j(z)$ is the probabilist's j -th Hermite polynomial, $\mu_j := \mathbb{E}_{z \sim \mathcal{N}(0,1)} [H_j(z) \sigma(z)]$ and $\tilde{\mu}_j := \mathbb{E}_{z \sim \mathcal{N}(0,1)} [H_j(z) \sigma_*(z)]$. Then, we have

$$\mathbb{E}_{(\mathbf{x}, y)} [\sigma(\hat{\mathbf{f}}_i^T \mathbf{x})y] = \mathbb{E}_{\mathbf{g}} \left[\sigma(\hat{\mathbf{f}}_i^T \mathbf{g}) \sigma_*(\hat{\boldsymbol{\xi}}^T \mathbf{g}) \right], \quad (104)$$

$$= \mathbb{E}_{z_i, z} \left[\sigma \left(\eta_i z + \sqrt{\|\hat{\mathbf{f}}_i\|^2 - \eta_i^2} z_i \right) \sigma_*(z) \right] \quad (105)$$

$$= \mathbb{E}_{z_i, z} \left[\left(\sum_{j=0}^{\infty} \frac{1}{j!} \mu_j H_j \left(\eta_i z + \sqrt{\|\hat{\mathbf{f}}_i\|^2 - \eta_i^2} z_i \right) \right) \left(\sum_{j=0}^{\infty} \frac{1}{j!} \tilde{\mu}_j H_j(z) \right) \right], \quad (106)$$

$$\stackrel{(a)}{=} \sum_{j=0}^{\infty} \frac{1}{(j!)^2} \mu_j \tilde{\mu}_j \mathbb{E}_{z_i, z} \left[H_j \left(\eta_i z + \sqrt{\|\hat{\mathbf{f}}_i\|^2 - \eta_i^2} z_i \right) H_j(z) \right] \quad (107)$$

$$\stackrel{(b)}{=} \sum_{j=0}^{\infty} \frac{1}{j!} \mu_j \tilde{\mu}_j \eta_i^j \stackrel{(c)}{=} \left(\sum_{j=0}^{l-1} \frac{1}{j!} \mu_j \tilde{\mu}_j \eta_i^j \right) + R_l \stackrel{(d)}{=} \mathbb{E}_{\mathbf{x}, y} [\hat{\sigma}_l(\hat{\mathbf{f}}_i^T \mathbf{x})y] + R_l, \quad (108)$$

where $R_i := \sum_{j=l}^{\infty} \frac{1}{j!} \mu_j \tilde{\mu}_j \eta_i^j$ to reach (c). To reach (a)-(b), we use the orthogonality of Hermite polynomials (Lemma 14). Finally, we get (d) by the definition of $\hat{\sigma}_l$. For $|R_i|$, we derive an upper bound as follows

$$|R_i| = \left| \sum_{j=l}^{\infty} \frac{1}{j!} \mu_j \tilde{\mu}_j \eta_i^j \right| \stackrel{(a)}{\leq} \sum_{j=l}^{\infty} \frac{1}{j!} |\mu_j \tilde{\mu}_j| |\eta_i^j| \stackrel{(b)}{\leq} \frac{C}{k}, \quad (109)$$

for some $C > 0$. The triangle inequality is used to reach (a) while we get (b) using $|\eta_i^l| = \mathcal{O}(1/k)$ (by the assumption of the lemma). Finally, we have

$$\left\| \mathbb{E}_{(\mathbf{x}, y)} [\sigma(\mathbf{F}\mathbf{x})y] - \mathbb{E}_{(\mathbf{x}, y)} [\hat{\sigma}_l(\mathbf{F}\mathbf{x})y] \right\| \leq \sqrt{\sum_{i=1}^k |\mathbb{E}[\sigma(\mathbf{f}_i^T \mathbf{x})y] - \mathbb{E}[\hat{\sigma}_l(\mathbf{f}_i^T \mathbf{x})y]|^2} = \sqrt{\sum_{i=1}^k R_i^2} \leq \frac{C}{\sqrt{k}},$$

which completes the proof. \square

REFERENCES

- Jimmy Ba, Murat A Erdogdu, Taiji Suzuki, Zhichao Wang, Denny Wu, and Greg Yang. High-dimensional asymptotics of feature learning: How one gradient step improves the representation. In *Advances in Neural Information Processing Systems*, 2022.
- Jimmy Ba, Murat A Erdogdu, Taiji Suzuki, Zhichao Wang, and Denny Wu. Learning in the presence of low-dimensional structure: A spiked random matrix perspective. In *Advances in Neural Information Processing Systems*, 2023.
- Jinho Baik, Gérard Ben Arous, and Sandrine Péché. Phase transition of the largest eigenvalue for nonnull complex sample covariance matrices. *The Annals of Probability*, 33(5):1643 – 1697, 2005.
- Mikhail Belkin, Daniel Hsu, Siyuan Ma, and Soumik Mandal. Reconciling modern machine-learning practice and the classical bias-variance trade-off. In *Proc. Natl. Acad. Sci.*, volume 116, pp. 15849–15854, 2019.
- David Bosch, Ashkan Panahi, and Babak Hassibi. Precise asymptotic analysis of deep random feature models. In *Conference on Learning Theory*, 2023.
- Hugo Cui, Luca Pesce, Yatin Dandi, Florent Krzakala, Yue Lu, Lenka Zdeborova, and Bruno Loureiro. Asymptotics of feature learning in two-layer networks after one gradient-step. In *International Conference on Machine Learning*, 2024.
- Alexandru Damian, Jason Lee, and Mahdi Soltanolkotabi. Neural networks can learn representations with gradient descent. In *Conference on Learning Theory*, 2022.
- Yatin Dandi, Florent Krzakala, Bruno Loureiro, Luca Pesce, and Ludovic Stephan. Learning two-layer neural networks, one (giant) step at a time. *arXiv preprint arXiv:2305.18270*, 2023a.
- Yatin Dandi, Ludovic Stephan, Florent Krzakala, Bruno Loureiro, and Lenka Zdeborova. Universality laws for gaussian mixtures in generalized linear models. In *Advances in Neural Information Processing Systems*, 2023b.
- Samet Demir and Zafer Dogan. Optimal nonlinearities improve generalization performance of random features. In *Asian Conference on Machine Learning*, 2024.
- Samet Demir and Zafer Dogan. Asymptotic analysis of two-layer neural networks after one gradient step under gaussian mixtures data with structure. In *International Conference on Learning Representations*, 2025.
- Oussama Dhifallah and Yue M Lu. A precise performance analysis of learning with random features. *arXiv preprint arXiv:2008.11904*, 2020.
- Elena Facco, Maria d’Errico, Alex Rodriguez, and Alessandro Laio. Estimating the intrinsic dimension of datasets by a minimal neighborhood information. *Scientific reports*, 7(1):12140, 2017.

- Mario Geiger, Arthur Jacot, Stefano Spigler, Franck Gabriel, Levent Sagun, Stéphane d’Ascoli, Giulio Biroli, Clément Hongler, and Matthieu Wyart. Scaling description of generalization with number of parameters in deep learning. *Journal of Statistical Mechanics: Theory and Experiment*, 2020(2):023401, feb 2020.
- Federica Gerace, Bruno Loureiro, Florent Krzakala, Marc Mézard, and Lenka Zdeborová. Generalisation error in learning with random features and the hidden manifold model. In *International Conference on Machine Learning*, 2020.
- Federica Gerace, Florent Krzakala, Bruno Loureiro, Ludovic Stephan, and Lenka Zdeborová. Gaussian universality of perceptrons with random labels. *Physical Review E*, 109(3):034305, 2024.
- Behrooz Ghorbani, Song Mei, Theodor Misiakiewicz, and Andrea Montanari. When do neural networks outperform kernel methods? *Advances in Neural Information Processing Systems*, 2020.
- Behrooz Ghorbani, Song Mei, Theodor Misiakiewicz, and Andrea Montanari. Linearized two-layers neural networks in high dimension. *The Annals of Statistics*, 49(2):1029 – 1054, 2021.
- Sebastian Goldt, Marc Mézard, Florent Krzakala, and Lenka Zdeborová. Modeling the influence of data structure on learning in neural networks: The hidden manifold model. *Physical Review X*, 10(4):041044, 2020.
- Sebastian Goldt, Bruno Loureiro, Galen Reeves, Florent Krzakala, Marc Mézard, and Lenka Zdeborová. The gaussian equivalence of generative models for learning with shallow neural networks. In *Mathematical and Scientific Machine Learning*, 2022.
- Hong Hu and Yue M Lu. Universality laws for high-dimensional learning with random features. *IEEE Transactions on Information Theory*, 69(3):1932–1964, Mar. 2023.
- Hong Hu, Yue M Lu, and Theodor Misiakiewicz. Asymptotics of random feature regression beyond the linear scaling regime. *arXiv preprint arXiv:2403.08160*, 2024.
- Iain M. Johnstone. On the distribution of the largest eigenvalue in principal components analysis. *The Annals of Statistics*, 29(2):295 – 327, 2001.
- W. F. Kibble. An extension of a theorem of mehler’s on hermite polynomials. *Mathematical Proceedings of the Cambridge Philosophical Society*, 41(1):12–15, 1945.
- Satish Babu Korada and Andrea Montanari. Applications of the lindeberg principle in communications and statistical learning. *IEEE Transactions on Information Theory*, 57(4):2440–2450, 2011.
- Alex Krizhevsky, Geoffrey Hinton, et al. Learning multiple layers of features from tiny images. Technical report, University of Toronto, 2009.
- Jarl Waldemar Lindeberg. Eine neue herleitung des exponentialgesetzes in der wahrscheinlichkeit-srechnung. *Mathematische Zeitschrift*, 15(1):211–225, 1922.
- Cosme Louart, Zhenyu Liao, and Romain Couillet. A random matrix approach to neural networks. *The Annals of Applied Probability*, 28(2):1190–1248, 2018.
- Yue M Lu and Horng-Tzer Yau. An equivalence principle for the spectrum of random inner-product kernel matrices with polynomial scalings. *The Annals of Applied Probability*, 35(4):2411–2470, 2025.
- Xiaoyi MAI and Zhenyu Liao. The breakdown of gaussian universality in classification of high-dimensional linear factor mixtures. In *International Conference on Learning Representations*, 2025.
- F Gustav Mehler. Ueber die entwicklung einer function von beliebig vielen variablen nach laplaceschen functionen höherer ordnung. 1866.

- Song Mei and Andrea Montanari. The generalization error of random features regression: Precise asymptotics and the double descent curve. *Communications on Pure and Applied Mathematics*, 75(4):667–766, 2022.
- Behrad Moniri, Donghwan Lee, Hamed Hassani, and Edgar Dobriban. A theory of non-linear feature learning with one gradient step in two-layer neural networks. In *International Conference on Machine Learning*, 2024.
- Andrea Montanari and Basil N Saeed. Universality of empirical risk minimization. In *Conference on Learning Theory*, 2022.
- Andrea Montanari, Feng Ruan, Youngtak Sohn, and Jun Yan. The generalization error of max-margin linear classifiers: High-dimensional asymptotics in the overparametrized regime. *arXiv preprint arXiv:1911.01544*, 2019.
- Alireza Mousavi-Hosseini, Denny Wu, Taiji Suzuki, and Murat A Erdogdu. Gradient-based feature learning under structured data. *Advances in Neural Information Processing Systems*, 2023.
- Preetum Nakkiran, Prayaag Venkat, Sham M. Kakade, and Tengyu Ma. Optimal regularization can mitigate double descent. In *International Conference on Learning Representations*, 2021.
- Ryan O’Donnell. *Analysis of Boolean Functions*. Cambridge University Press, 2014.
- Luca Pesce, Florent Krzakala, Bruno Loureiro, and Ludovic Stephan. Are gaussian data all you need? the extents and limits of universality in high-dimensional generalized linear estimation. In *International Conference on Machine Learning*, 2023.
- Ali Rahimi and Benjamin Recht. Random features for large-scale kernel machines. In *Advances in Neural Information Processing Systems*, 2007.
- Dominik Schröder, Hugo Cui, Daniil Dmitriev, and Bruno Loureiro. Deterministic equivalent and error universality of deep random features learning. In *International Conference on Machine Learning*, 2023.
- Stefano Spigler, Mario Geiger, and Matthieu Wyart. Asymptotic learning curves of kernel methods: empirical data versus teacher–student paradigm. *Journal of Statistical Mechanics: Theory and Experiment*, 2020(12):124001, 2020.
- Michel Talagrand. *Mean field models for spin glasses: Volume I: Basic examples*, volume 54. Springer Science & Business Media, 2010.
- Roman Vershynin. *High-dimensional probability: An introduction with applications in data science*, volume 47. Cambridge University Press, 2018.
- Jianxin Wang and José Bento. Optimal activation functions for the random features regression model. In *International Conference on Learning Representations*, 2022.
- Garrett G Wen, Hong Hu, Yue M Lu, Zhou Fan, and Theodor Misiakiewicz. When does gaussian equivalence fail and how to fix it: Non-universal behavior of random features with quadratic scaling. *arXiv preprint arXiv:2512.03325*, 2025.
- Jacob Zavatone-Veth and Cengiz Pehlevan. Learning curves for deep structured gaussian feature models. *Advances in Neural Information Processing Systems*, 2023.

SUPPLEMENTARY MATERIALS

SM1 AUXILIARY RESULTS FOR THE PROOFS

In this section, we provide auxiliary results that are used in the proofs given in the previous sections.

Lemma SM1. *Suppose assumptions (S.1)-(S.6) in Section 3 and additional assumptions S.7-S.8 in Appendix A. Then,*

$$\mathcal{G}_\sigma \xrightarrow{\mathbb{P}} e_{\mathcal{G}} \quad \text{if and only if} \quad \mathcal{G}_{\hat{\sigma}} \xrightarrow{\mathbb{P}} e_{\mathcal{G}}, \quad (\text{SM1})$$

if the following holds,

$$\frac{\Phi_{\mathbf{A}}(\tau_1, \tau_2)}{k} \xrightarrow{\mathbb{P}} \phi \quad \text{if and only if} \quad \frac{\Phi_{\mathbf{B}}(\tau_1, \tau_2)}{k} \xrightarrow{\mathbb{P}} \phi, \quad (\text{SM2})$$

where $\Phi_{\mathbf{R}}(\tau_1, \tau_2)$ is the perturbed problem defined in (18). Also, $\mathbf{A} := [\mathbf{a}_1, \mathbf{a}_2, \dots, \mathbf{a}_m]^T$ and $\mathbf{B} := [\mathbf{b}_1, \mathbf{b}_2, \dots, \mathbf{b}_m]^T$ where $\mathbf{a}_i := \sigma(\mathbf{F}\mathbf{x}_i)$ and $\mathbf{b}_i := \hat{\sigma}(\mathbf{F}\mathbf{x}_i)$ for all $i \in \{1, 2, \dots, m\}$.

Proof. We start by writing \mathcal{G}_σ as follows

$$\mathcal{G}_\sigma := \mathbb{E}_{(\mathbf{x}, y)} (y - \hat{\omega}_\sigma^T \sigma(\mathbf{F}\mathbf{x}))^2, \quad (\text{SM3})$$

$$= \mathbb{E}[y^2] - 2\hat{\omega}_\sigma^T \mathbb{E}[\sigma(\mathbf{F}\mathbf{x})y] + \hat{\omega}_\sigma^T \mathbb{E}[\sigma(\mathbf{F}\mathbf{x})\sigma(\mathbf{F}\mathbf{x})^T] \hat{\omega}_\sigma, \quad (\text{SM4})$$

$$= \mathbb{E}[y^2] - 2\hat{\omega}_\sigma^T \Sigma_{xy} + \hat{\omega}_\sigma^T \Sigma_x \hat{\omega}_\sigma, \quad (\text{SM5})$$

$$= \mathbb{E}[y^2] - 2\pi_{\mathbf{A}} + \rho_{\mathbf{A}}, \quad (\text{SM6})$$

where we define $\pi_{\mathbf{A}} := \hat{\omega}_0^T \Sigma_{xy}$ and $\rho_{\mathbf{A}} := \hat{\omega}_0^T \Sigma_x \hat{\omega}_0$ in the last step. Note that $\hat{\omega}_\sigma = \hat{\omega}_0$ and $\hat{\omega}_{\hat{\sigma}} = \hat{\omega}_m$ by definition (25). Similarly, we can arrive at $\mathcal{G}_{\hat{\sigma}} = \mathbb{E}[y^2] - 2\pi_{\mathbf{B}} + \rho_{\mathbf{B}} + R$ for activation function $\hat{\sigma}$ where $\pi_{\mathbf{B}} := \hat{\omega}_m^T \Sigma_{xy}$ and $\rho_{\mathbf{B}} := \hat{\omega}_m^T \Sigma_x \hat{\omega}_m$. Furthermore, we define R as the remainder term as follows

$$R := \hat{\omega}_m^T (\mathbb{E}[\hat{\sigma}(\mathbf{F}\mathbf{x})\hat{\sigma}(\mathbf{F}\mathbf{x})^T] - \Sigma_x) \hat{\omega}_m - 2\hat{\omega}_m^T (\mathbb{E}[\hat{\sigma}(\mathbf{F}\mathbf{x})y] - \Sigma_{xy}), \quad (\text{SM7})$$

which can be bounded as

$$\mathbb{E}_{\mathbf{F}} |R| \leq \mathbb{E}_{\mathbf{F}} \left(\|\hat{\omega}_m\|^2 \right) \left\| \mathbb{E}[\hat{\sigma}(\mathbf{F}\mathbf{x})\hat{\sigma}(\mathbf{F}\mathbf{x})^T] - \Sigma_x \right\| + 2\mathbb{E}_{\mathbf{F}} (\|\hat{\omega}_m\|) \|\mathbb{E}[\hat{\sigma}(\mathbf{F}\mathbf{x})y] - \Sigma_{xy}\|, \quad (\text{SM8})$$

$$= o(1), \quad (\text{SM9})$$

where we use a bound on $\mathbb{E}_{\mathbf{F}} [\|\hat{\omega}_m\|^l]$ (Lemma SM9) with the equivalence of covariance matrices (6) and the equivalence of cross-covariance vectors (7) to reach the last line. Now, to prove (SM1), we need to show $\rho_{\mathbf{A}} \xrightarrow{\mathbb{P}} \rho^* = \frac{\partial}{\partial \tau_1} q^*(0, 0)$ while $\rho_{\mathbf{B}} \xrightarrow{\mathbb{P}} \rho^*$ and $\pi_{\mathbf{A}} \xrightarrow{\mathbb{P}} \pi^* = \frac{\partial}{\partial \tau_2} q^*(0, 0)$ while $\pi_{\mathbf{B}} \xrightarrow{\mathbb{P}} \pi^*$ under assumption S.8. We show $\rho_{\mathbf{A}} \xrightarrow{\mathbb{P}} \rho^*$ in the following while the rest can be shown analogously. First, observe that, for any $\tau_1, \tau_2 \in (-\tau_*, \tau_*)$,

$$\Phi_{\mathbf{A}}(\tau_1, \tau_2) \leq \Phi_{\mathbf{A}}(0, 0) + \tau_1 k \hat{\omega}_0^T \Sigma_x \hat{\omega}_0 + \tau_2 k \hat{\omega}_0^T \Sigma_{xy}, \quad (\text{SM10})$$

which we arrive at by using the definition of the perturbed optimization (18). Then, for any $\tau \in (0, \tau_*)$,

$$\frac{\Phi_{\mathbf{A}}(\tau, 0) - \Phi_{\mathbf{A}}(0, 0)}{k\tau} \leq \rho_{\mathbf{A}} \leq \frac{\Phi_{\mathbf{A}}(-\tau, 0) - \Phi_{\mathbf{A}}(0, 0)}{-k\tau}. \quad (\text{SM11})$$

For a fixed $\epsilon > 0$, there exists $\delta > 0$ such that

$$\left| \frac{q^*(\delta, 0) - q^*(0, 0)}{\delta} - \rho^* \right| \leq \epsilon/3, \quad (\text{SM12})$$

due to assumption S.8 in Appendix A. Focusing on the inequality on the left in (SM11), we get:

$$\mathbb{P}(\rho_{\mathbf{A}} - \rho^* < -\epsilon) \leq \mathbb{P} \left(\frac{\Phi_{\mathbf{A}}(\delta, 0) - \Phi_{\mathbf{A}}(0, 0)}{k\delta} - \rho^* < -\epsilon \right), \quad (\text{SM13})$$

$$\leq \mathbb{P}(|\Phi_{\mathbf{A}}(\delta, 0)/k - q^*(\delta, 0)| > \delta\epsilon/3) + \mathbb{P}(|\Phi_{\mathbf{A}}(0, 0)/k - q^*(0, 0)| > \delta\epsilon/3), \quad (\text{SM14})$$

$$= 0, \quad (\text{SM15})$$

where we use (SM12) in the middle line and $\Phi_{\mathbf{A}}(\tau_1, \tau_2)/k \xrightarrow{\mathbb{P}} q^*(\tau_1, \tau_2)$ is used in the last line. Applying the same steps to the inequality on the right in (SM11), we arrive at $\mathbb{P}(\rho_{\mathbf{A}} - \rho^* > \epsilon) = 0$. Therefore, we conclude that $\rho_{\mathbf{A}} \xrightarrow{\mathbb{P}} \rho^*$. Using the same reasoning that we used to show $\rho_{\mathbf{A}} \xrightarrow{\mathbb{P}} \rho^*$, we may also show $\rho_{\mathbf{B}} \xrightarrow{\mathbb{P}} \rho^*$, $\pi_{\mathbf{A}} \xrightarrow{\mathbb{P}} \pi^*$, and $\pi_{\mathbf{B}} \xrightarrow{\mathbb{P}} \pi^*$ but we omit them here. Since we have $\rho_{\mathbf{A}} \xrightarrow{\mathbb{P}} \rho^*$, $\rho_{\mathbf{B}} \xrightarrow{\mathbb{P}} \rho^*$, $\pi_{\mathbf{A}} \xrightarrow{\mathbb{P}} \pi^*$, and $\pi_{\mathbf{B}} \xrightarrow{\mathbb{P}} \pi^*$, we reach (SM1) by using (SM6). \square

Lemma SM2. *Suppose the setting in Appendix A. Then, for any $\phi \in \mathbb{R}$,*

$$\frac{\Phi_{\mathbf{A}}(\tau_1, \tau_2)}{k} \xrightarrow{\mathbb{P}} \phi \quad \text{if and only if} \quad \frac{\Phi_{\mathbf{B}}(\tau_1, \tau_2)}{k} \xrightarrow{\mathbb{P}} \phi, \quad (\text{SM16})$$

if the following holds:

$$\left| \mathbb{E} \varphi \left(\frac{1}{k} \Phi_{\mathbf{A}} \right) - \mathbb{E} \varphi \left(\frac{1}{k} \Phi_{\mathbf{B}} \right) \right| \leq \max \{ \|\varphi\|_{\infty}, \|\varphi'\|_{\infty}, \|\varphi''\|_{\infty} \} \kappa_k, \quad (\text{SM17})$$

for some $\kappa_k = o(1)$ and every bounded test function $\varphi(x)$ which has bounded first two derivatives.

Proof. The proof is adapted from Section II-D in Hu & Lu (2023). We need to select an appropriate test function to start the proof. For any fixed $\epsilon > 0$ and ϕ , let

$$\varphi_{\epsilon}(x) := \mathbb{1}_{|x| \geq 3\epsilon/2} * \zeta_{\epsilon/2}(x - \phi), \quad (\text{SM18})$$

where $*$ denotes the convolution operation and $\zeta_{\epsilon}(x) := \epsilon^{-1} \zeta(x/\epsilon)$ is a scaled mollifier. We define a standard mollifier as:

$$\zeta(x) := \begin{cases} ce^{-1/(1-x^2)}, & \text{if } |x| < 1, \\ 0, & \text{otherwise,} \end{cases} \quad (\text{SM19})$$

for some constant c ensuring $\int_{\mathbb{R}} \zeta(x) dx = 1$. We may easily verify that $\|\varphi'_{\epsilon}(x)\|_{\infty} < C/\epsilon$ and $\|\varphi''_{\epsilon}(x)\|_{\infty} < C/\epsilon^2$ for some constant C . Furthermore,

$$\mathbb{1}_{|x-\phi| \geq 2\epsilon} \leq \varphi_{\epsilon}(x) \leq \mathbb{1}_{|x-\phi| \geq \epsilon}. \quad (\text{SM20})$$

Let $x = \Phi_{\mathbf{A}}/k$ in (SM20) and take the expectation:

$$\mathbb{P}(|\Phi_{\mathbf{A}}/k - \phi| \geq 2\epsilon) \leq \mathbb{E}[\varphi_{\epsilon}(\Phi_{\mathbf{A}}/k)]. \quad (\text{SM21})$$

Similarly, let $x = \Phi_{\mathbf{B}}/k$ in (SM20) and take the expectation:

$$\mathbb{E}[\varphi_{\epsilon}(\Phi_{\mathbf{B}}/k)] \leq \mathbb{P}(|\Phi_{\mathbf{B}}/k - \phi| \geq \epsilon). \quad (\text{SM22})$$

Using (SM17) together with the last two equations, we arrive at

$$\mathbb{P}(|\Phi_{\mathbf{A}}/k - \phi| \geq 2\epsilon) \leq \mathbb{P}(|\Phi_{\mathbf{B}}/k - \phi| \geq \epsilon) + \max \{ C, C/\epsilon, C/\epsilon^2 \} \kappa_k, \quad (\text{SM23})$$

which leads to

$$\mathbb{P}(|\Phi_{\mathbf{A}}/k - \phi| \geq 2\epsilon) \leq \mathbb{P}(|\Phi_{\mathbf{B}}/k - \phi| \geq \epsilon) + \frac{C\kappa_k}{\epsilon^2}, \quad (\text{SM24})$$

for $\epsilon \in (0, 1)$ satisfying $\kappa_k/\epsilon^2 = o(1)$. Applying the same steps after switching \mathbf{A} with \mathbf{B} , we get

$$\mathbb{P}(|\Phi_{\mathbf{B}}/k - \phi| \geq 2\epsilon) \leq \mathbb{P}(|\Phi_{\mathbf{A}}/k - \phi| \geq \epsilon) + \frac{C\kappa_k}{\epsilon^2}. \quad (\text{SM25})$$

Combining the last two results and letting $\epsilon \rightarrow 0^+$ with $\kappa_k/\epsilon^2 = o(1)$, we reach (SM16). \square

Lemma SM3. *Suppose the definitions in Appendix A. Then, the following holds:*

$$\Phi_{t-1} = \Psi_t(\mathbf{a}_t), \quad \text{and} \quad \Phi_t = \Psi_t(\mathbf{b}_t). \quad (\text{SM26})$$

Proof. We apply Taylor expansion to Φ_{t-1} around $\Phi_{\setminus t}$:

$$\Phi_{t-1} = \Phi_{\setminus t} + \min_{\omega \in \mathbb{R}^k} \left\{ (\omega - \hat{\omega}_{\setminus t})^T \mathbf{d}_{\setminus t} + \frac{1}{2} (\omega - \hat{\omega}_{\setminus t})^T \mathbf{H}_{\setminus t} (\omega - \hat{\omega}_{\setminus t}) + (\omega^T \mathbf{a}_t - y_t)^2 \right\}, \quad (\text{SM27})$$

where $\mathbf{d}_{\setminus t}$ and $\mathbf{H}_{\setminus t}$ are respectively gradient vector and Hessian matrix of $\Phi_{\setminus t}$ evaluated at $\hat{\omega}_{\setminus t}$. Note that we do not need higher order terms since $\Phi_{\setminus t}$ only involves quadratic terms, which means higher order terms are equal to 0. Furthermore, the gradient vector $\mathbf{d}_{\setminus t}$ is equal to 0 due to the first-order optimality condition in (29). This leads us to:

$$\Phi_{t-1} = \Phi_{\setminus t} + \min_{\omega \in \mathbb{R}^k} \left\{ \frac{1}{2} (\omega - \hat{\omega}_{\setminus t})^T \mathbf{H}_{\setminus t} (\omega - \hat{\omega}_{\setminus t}) + (\omega^T \mathbf{a}_t - y_t)^2 \right\} = \Psi_t(\mathbf{a}_t). \quad (\text{SM28})$$

Similarly, one can show $\Phi_t = \Psi_t(\mathbf{b}_t)$ using the same reasoning, which is omitted here. \square

Lemma SM4. *Suppose the definitions in Appendix A. For some ϵ , the following holds:*

$$\max \left\{ \mathbb{E}_{\setminus \mathbf{F}} (\Psi_t(\mathbf{b}_t) - \Phi_{\setminus t})^2, \mathbb{E}_{\setminus \mathbf{F}} (\Psi_t(\mathbf{a}_t) - \Phi_{\setminus t})^2 \right\} \leq k^{1-\epsilon} \text{polylog } k. \quad (\text{SM29})$$

Proof. Let $\mathbf{r}_t = \mathbf{a}_t$ or $\mathbf{r}_t = \mathbf{b}_t$. Then,

$$\mathbb{E}_{\setminus \mathbf{F}} (\Psi_t(\mathbf{r}_t) - \Phi_{\setminus t})^2 \leq \mathbb{E}_{\setminus \mathbf{F}} \left(\hat{\omega}_{\setminus t}^T \mathbf{r}_t - y_t \right)^4, \quad (\text{SM30})$$

$$\leq \sqrt{\mathbb{E}_{\setminus \mathbf{F}} \left(\left| \hat{\omega}_{\setminus t}^T \mathbf{r}_t \right| + 1 \right)^8} \text{polylog } k, \quad (\text{SM31})$$

$$\leq Q(\|\hat{\omega}_{\setminus t}\|) \|\hat{\mathbf{F}}\|^4 \text{polylog } k, \quad (\text{SM32})$$

$$\leq k^{1-\epsilon} \text{polylog } k \quad (\text{SM33})$$

where $Q(x)$ is some finite-degree polynomial, $\hat{\mathbf{F}} := \mathbf{F}(\mathbf{I}_n + (\sqrt{1+\theta} - 1)\gamma\gamma^T)$ and some $\epsilon > 0$ satisfying $\theta^2 \leq n^{1-\epsilon}$. We use (37) in the first step. Then, we reach the second line using Lemma SM5. In the third step, we use Lemma SM6. Finally, we use (55) and Lemma 8 to conclude the proof. \square

Lemma SM5. *Suppose the definitions in Appendix A. Then, the following holds:*

$$\mathbb{E}_{\setminus \mathbf{F}} \left(\hat{\omega}_{\setminus t}^T \mathbf{r} - y_t \right)^{2l} \leq \sqrt{\mathbb{E}_{\setminus \mathbf{F}} \left(\left| \hat{\omega}_{\setminus t}^T \mathbf{r} \right| + 1 \right)^{4l}} \text{polylog } k, \quad (\text{SM34})$$

for $l \in \mathbb{Z}^+$.

Proof. Let $y_t := \sigma_*(s_t)$ where $s_t := \frac{\xi^T \mathbf{x}_t}{\sqrt{1+\theta\alpha^2}}$. Then, for any $x \in \mathbb{R}$,

$$(x - y_t)^2 \leq |x|^2 + 2|x||y_t| + |y_t|^2, \quad (\text{SM35})$$

$$\leq |x|^2 + 2|x|C(|s_t|^K + 1) + C^2(|s_t|^K + 1)^2, \quad (\text{SM36})$$

$$\leq \hat{C}(|x| + 1)^2(|s_t|^K + 1)^2, \quad (\text{SM37})$$

for some $C, \hat{C} > 0$. To reach the second line, we use $|y_t| \leq C(|s_t|^K + 1)$ due to assumption (S.3). Using this result, we get:

$$\mathbb{E}_{\setminus \mathbf{F}} \left(\hat{\omega}_{\setminus t}^T \mathbf{r} - y_t \right)^{2l} \leq \hat{C}^l \mathbb{E}_{\setminus \mathbf{F}} \left[\left(\left| \hat{\omega}_{\setminus t}^T \mathbf{r} \right| + 1 \right)^{2l} \left(|s_t|^K + 1 \right)^{2l} \right], \quad (\text{SM38})$$

$$\leq \hat{C}^l \sqrt{\mathbb{E}_{\setminus \mathbf{F}} \left(\left| \hat{\omega}_{\setminus t}^T \mathbf{r} \right| + 1 \right)^{4l}} \sqrt{\mathbb{E}_{\setminus \mathbf{F}} \left(|s_t|^K + 1 \right)^{4l}}. \quad (\text{SM39})$$

$s_t \sim \mathcal{N}(0, 1)$ so $\mathbb{P}(|s_t| > \epsilon) \leq 2e^{-\epsilon^2/2}$ (Vershynin, 2018, Eq. (2.10)). Therefore, we can reach (SM34) by using moment bounds for $|s_t|$ from Lemma SM7. \square

Lemma SM6. *Suppose assumptions (S.1)-(S.6). Let $\mathbf{a} := \sigma(\mathbf{F}\mathbf{x})$. Furthermore, let $\hat{\mathbf{F}} := \mathbf{F}(\mathbf{I}_n + (\sqrt{1+\theta} - 1)\gamma\gamma^T)$. Then, there exist some $c, C > 0$ such that the following holds*

$$\mathbb{P}_{\setminus \mathbf{F}} \left(\left| \omega^T \mathbf{a} \right| \geq \epsilon \right) \leq 2e^{-\frac{\epsilon^2}{c\|\omega\|^2 \|\hat{\mathbf{F}}\|^2 \text{polylog } k}}, \quad (\text{SM40})$$

$$\mathbb{E}_{\setminus \mathbf{F}} \left(\left| \omega^T \mathbf{a} \right|^l \right) \leq (l!) \left(C\|\omega\|^2 \|\hat{\mathbf{F}}\|^2 \text{polylog } k \right)^{l/2}, \quad (\text{SM41})$$

for any $l \in \mathbb{Z}^+$, any fixed $\omega \in \mathbb{R}^k$ and $\epsilon \geq 0$.

Proof. Let $\mathbf{g} \sim \mathcal{N}(0, \mathbf{I}_k)$. One can verify that the function $f(\mathbf{g}) := \boldsymbol{\omega}^T \mathbf{a} = \boldsymbol{\omega}^T \sigma(\hat{\mathbf{F}}\mathbf{g})$ is $(\|\sigma'\|_\infty \|\boldsymbol{\omega}\| \|\hat{\mathbf{F}}\|)$ -Lipschitz continuous. Furthermore, $\mathbb{E}_{\mathbf{F}}(\boldsymbol{\omega}^T \mathbf{a}) = 0$ due to $\sigma(x)$ being an odd function. Furthermore, $\sigma'(z) \leq \text{polylog } k$ with high probability for $z \sim \mathcal{N}(0, \hat{C})$ with all $\hat{C} > 0$, which allows us to continue with $\|\sigma'\|_\infty \leq \text{polylog } k$ by using a truncation argument (similar to Lemma 13). Therefore, we can reach (SM40)-(SM41) using Lemma SM7. \square

Lemma SM7 (Concentration of Lipschitz Functions - (Hu & Lu, 2023, Theorem 3)). *Consider $\mathbf{g} \sim \mathcal{N}(0, \mathbf{I}_k)$. Then, for any κ -Lipschitz function $f : \mathbb{R}^k \rightarrow \mathbb{R}$ and $\epsilon \geq 0$,*

$$\mathbb{P}(|f(\mathbf{g}) - \mathbb{E}[f(\mathbf{g})]| \geq \epsilon) \leq 2e^{-\epsilon^2/(4\kappa^2)}. \quad (\text{SM42})$$

Furthermore, let x be a random variable. If x satisfying $\mathbb{P}(|x| > v) \leq ce^{-Cv}$ for some $C, c > 0$,

$$\mathbb{E}[|x|^l] \leq clC^{-l} \int_0^\infty e^{-v} v^{l-1} dv = c(l!)C^{-l} \quad \text{for any } l \in \mathbb{Z}^+. \quad (\text{SM43})$$

Similarly, if x satisfying $\mathbb{P}(|x| > v) \leq ce^{-Cv^2}$ for some $C, c > 0$,

$$\mathbb{E}[|x|^l] \leq 2c(l!)C^{-l/2} \quad \text{for any } l \in \mathbb{Z}^+. \quad (\text{SM44})$$

Proof. See (Talagrand, 2010, Theorem 1.3.4). \square

Lemma SM8. *Suppose the definitions in Appendix A. Let $\epsilon > 0$ be a constant satisfying $\theta \leq n^{1/2-\epsilon/2}$. For $\mathbf{r}_t = \mathbf{a}_t$ or $\mathbf{r}_t = \mathbf{b}_t$, we have*

$$\mathbb{P}(|\nu_t(\mathbf{r}_t) - \mathbb{E}_t[\nu_t(\mathbf{r}_t)]| > \delta) \leq ce^{-Ck^\epsilon \delta^2 / \text{polylog } k}, \quad (\text{SM45})$$

for some $c, C > 0$. Furthermore,

$$\mathbb{E}_t[|\nu_t(\mathbf{r}_t) - \mathbb{E}_t[\nu_t(\mathbf{r}_t)]|^l] \leq 2c(l!)(Ck^\epsilon / \text{polylog } k)^{-l/2}, \quad (\text{SM46})$$

for some $c, C > 0$ and any $l \in \mathbb{Z}^+$. Finally,

$$\left| \mathbb{E}_t \nu_t(\mathbf{a}_t) - \mathbb{E}_t \nu_t(\mathbf{b}_t) \right| = \mathcal{O}(k^{-\varsigma}), \quad (\text{SM47})$$

for some $\varsigma > 0$.

Proof. Consider

$$\nu_t(\mathbf{r}_t) = \mathbf{r}_t^T \mathbf{H}_{\sqrt{t}}^{-1} \mathbf{r}_t = \frac{\mathbf{r}_t^T \bar{\mathbf{H}}_{\sqrt{t}}^{-1} \mathbf{r}_t}{k}, \quad (\text{SM48})$$

where $\bar{\mathbf{H}}_{\sqrt{t}}$ is defined as follows to take the $1/k$ scaling out

$$\bar{\mathbf{H}}_{\sqrt{t}} := \frac{2}{k} \sum_{i=1}^{t-1} \mathbf{b}_i \mathbf{b}_i^T + \frac{2}{k} \sum_{i=t+1}^m \mathbf{a}_i \mathbf{a}_i^T + \frac{1}{k} \nabla^2 Q(\hat{\boldsymbol{\omega}}_{\sqrt{t}}). \quad (\text{SM49})$$

Then, using s -strong convexity of $Q(\boldsymbol{\omega})/m$ due to assumption S.7, we have $\bar{\mathbf{H}}_{\sqrt{t}} \succeq (m/k)s\mathbf{I}_k$, which lead to $\|\bar{\mathbf{H}}_{\sqrt{t}}^{-1}\| \leq (k/m)(1/s)$. Furthermore, we can rewrite $\mathbf{a}_i = \sigma(\mathbf{F}\mathbf{x}_i)$ equivalently as $\sigma(\hat{\mathbf{F}}\mathbf{g})$ for $\hat{\mathbf{F}} := \mathbf{F}(\mathbf{I}_n + (\sqrt{1+\theta}-1)\boldsymbol{\gamma}\boldsymbol{\gamma}^T)$ and $\mathbf{g} \sim \mathcal{N}(0, \mathbf{I}_n)$. We have $\|\hat{\mathbf{F}}\| \leq k^{1/4-\epsilon/4} \text{polylog } k$ (for some $\epsilon > 0$ satisfying $\theta \leq n^{1/2-\epsilon/2}$), which is due to (55). Furthermore, we have $\|\sigma'\|_\infty \leq \text{polylog } k$ by using a truncation argument (similar to Lemma 13) as mentioned in the proof of Lemma SM6. Then, we use (Louart et al., 2018, Lemma 1) with the bounds for $\|\hat{\mathbf{F}}\|$ and $\|\bar{\mathbf{H}}_{\sqrt{t}}^{-1}\|$ to reach (SM45). Finally, (SM46) can be obtained using Lemma SM7. To show (SM47), we proceed as

$$\left| \mathbb{E}_t \nu_t(\mathbf{a}_t) - \mathbb{E}_t \nu_t(\mathbf{b}_t) \right| = \frac{1}{k} \left| \mathbb{E}_t \left[\mathbf{a}_t^T \bar{\mathbf{H}}_{\sqrt{t}}^{-1} \mathbf{a}_t \right] - \mathbb{E}_t \left[\mathbf{b}_t^T \bar{\mathbf{H}}_{\sqrt{t}}^{-1} \mathbf{b}_t \right] \right|, \quad (\text{SM50})$$

$$= \frac{1}{k} \left| \text{Tr} \left(\bar{\mathbf{H}}_{\sqrt{t}}^{-1} \left(\mathbb{E}_t [\mathbf{a}_t \mathbf{a}_t^T] - \mathbb{E}_t [\mathbf{b}_t \mathbf{b}_t^T] \right) \right) \right|, \quad (\text{SM51})$$

$$= \mathcal{O}(k^{-\varsigma}), \quad (\text{SM52})$$

for some $\varsigma > 0$, where Tr denotes the trace while we use $\|\bar{\mathbf{H}}_{\sqrt{t}}^{-1}\| \leq (k/m)(1/s)$ and (6) to reach the last line. \square

Lemma SM9. *Suppose the definitions in Appendix A. Then, the following holds:*

$$\mathbb{E}_{\setminus \mathbf{F}} \|\hat{\omega}_t\|^l \leq \text{polylog } k, \quad (\text{SM53})$$

$$\mathbb{E}_{\setminus \mathbf{F}} \|\hat{\omega}_{\setminus t}\|^l \leq \text{polylog } k, \quad (\text{SM54})$$

for any $l \in \mathbb{Z}^+$ and any $t \in \{0, \dots, m\}$.

Proof. We show (SM53) here while (SM54) can be proved similarly. Let $\mathbf{r}_i := \mathbf{b}_i$ for $i \in \{1, \dots, k\}$ and $\mathbf{r}_i := \mathbf{a}_i$ for $t \in \{k+1, \dots, m\}$. Furthermore, let $Q(\omega) := m\lambda \|\omega\|_2^2 + \tau_1 k \omega^T \Sigma_x \omega + \tau_2 k \omega^T \Sigma_{xy}$. Then,

$$\frac{1}{m} Q(\hat{\omega}_t) \leq \frac{1}{m} \sum_{i=1}^m (\hat{\omega}_t^T \mathbf{r}_i - y_i)^2 + \frac{1}{m} Q(\hat{\omega}_t) \leq \frac{1}{m} \sum_{i=1}^m y_i^2 + \frac{1}{m} Q(\mathbf{0}), \quad (\text{SM55})$$

since $\hat{\omega}_t$ is the optimal solution defined in (25). Furthermore, $Q(\omega)/m$ is s -strongly convex by assumption S.7 in Appendix A. Using this fact, we reach

$$\frac{1}{m} Q(\hat{\omega}_t) \geq \frac{1}{m} Q(\mathbf{0}) + \frac{1}{m} \nabla Q(\mathbf{0})^T \hat{\omega}_t + (s/2) \|\hat{\omega}_t\|^2, \quad (\text{SM56})$$

$$\geq \frac{1}{m} Q(\mathbf{0}) - \frac{1}{m} \|\nabla Q(\mathbf{0})\| \|\hat{\omega}_t\| + (s/2) \|\hat{\omega}_t\|^2. \quad (\text{SM57})$$

We may then combine the found lower and upper bounds for $Q(\hat{\omega}_t)/m$ as follows:

$$(s/2) \|\hat{\omega}_t\|^2 - \frac{1}{m} \|\nabla Q(\mathbf{0})\| \|\hat{\omega}_t\| \leq \frac{1}{m} \sum_{i=1}^m y_i^2, \quad (\text{SM58})$$

which leads to

$$\|\hat{\omega}_t\| \leq \frac{\|\nabla Q(\mathbf{0})\|/m + \sqrt{\|\nabla Q(\mathbf{0})\|^2/m^2 + 2(s/m) \sum_{i=1}^m y_i^2}}{s}, \quad (\text{SM59})$$

$$\leq \frac{2\|\nabla Q(\mathbf{0})\|/m + \sqrt{2(s/m) \sum_{i=1}^m y_i^2}}{s}, \quad (\text{SM60})$$

$$\leq \left(\frac{1}{m} \sum_{i=1}^m y_i^2 \right)^{1/2} \text{polylog } k, \quad (\text{SM61})$$

where we use $\|\nabla Q(\mathbf{0})\|/m = |\tau_2|(k/m) \|\Sigma_{xy}\| \leq \text{polylog } k$ since we have $(k/m) \in (0, \infty)$ by assumption (S.4) in Section 3, $\tau_2 = \mathcal{O}(1/\sqrt{k})$ by assumption S.7 in Appendix A and one can easily show $\|\Sigma_{xy}\| \leq \sqrt{k} \text{polylog } k$ using (108). Then, we consider l -th power of $\|\hat{\omega}_t\|$ as

$$\|\hat{\omega}_t\|^l \leq \left(\frac{1}{m} \sum_{i=1}^m y_i^2 \right)^{l/2} \text{polylog } k. \quad (\text{SM62})$$

Let $y_i := \sigma_*(s_i)$ where $s_i := \frac{\xi^T \mathbf{x}_i}{\sqrt{1+\theta\alpha^2}}$. Using $|y_i| \leq C(|s_i|^K + 1)$ due to assumption (S.3), we get

$$\mathbb{E}_{\setminus \mathbf{F}} \|\hat{\omega}_t\|^l \leq \mathbb{E}_{\setminus \mathbf{F}} \left(\frac{1}{m} \sum_{i=1}^m (|s_i|^K + 1)^2 \right)^{l/2} \text{polylog } k. \quad (\text{SM63})$$

Finally, $s_i \sim \mathcal{N}(0, 1)$ so we reach (SM53) by using moment bounds for $|s_i|$ from Lemma SM7. Similarly, (SM54) can shown using analogous steps. \square

Lemma SM10. *Let $f : \mathbb{R} \rightarrow \mathbb{R}$ be a function satisfying $|f(x)| \leq C(1 + |x|^K)$ for all $x \in \mathbb{R}$ and some constants $C > 0, K \in \mathbb{Z}^+$. Furthermore, define a truncated version of f as*

$$f_\epsilon(x) := \begin{cases} f(x), & \text{if } |x| < \epsilon, \\ 0, & \text{otherwise,} \end{cases} \quad (\text{SM64})$$

for $\epsilon > 0$. If $\epsilon = 2\log k$, the following holds for any constant $a > 0$ and $z \sim \mathcal{N}(0, 1)$,

$$\mathbb{E}_z |f(az) - f_\epsilon(az)| = \frac{\text{polylog } k}{k^{\log k}}. \quad (\text{SM65})$$

Proof. We start by using $1 = \mathbb{1}_{|z| < \epsilon} + \mathbb{1}_{|z| \geq \epsilon}$ as follows

$$\mathbb{E}_z |f(az) - f_\epsilon(az)| \leq \mathbb{E}_z [|f(az) - f_\epsilon(az)| (\mathbb{1}_{|z| < \epsilon} + \mathbb{1}_{|z| \geq \epsilon})], \quad (\text{SM66})$$

$$= \mathbb{E}_z [|f(az) - f_\epsilon(az)| \mathbb{1}_{|z| \geq \epsilon}], \quad (\text{SM67})$$

$$= \mathbb{E}_z [|f(az)| \mathbb{1}_{|z| \geq \epsilon}] \quad (\text{SM68})$$

$$\stackrel{(a)}{\leq} \sqrt{\mathbb{E}_z [f(az)^2]} \sqrt{\mathbb{E}_z [(\mathbb{1}_{|z| \geq \epsilon})^2]}, \quad (\text{SM69})$$

$$= \sqrt{\mathbb{E}_z [f(az)^2]} \sqrt{\mathbb{P}(|z| \geq \epsilon)}, \quad (\text{SM70})$$

$$\stackrel{(b)}{\leq} C \sqrt{\mathbb{E}_z [(a^{2K} z^{2K} + 2a^K |z|^K + 1)]} \sqrt{2e^{-\epsilon^2/2}}, \quad (\text{SM71})$$

$$\stackrel{(c)}{\leq} \frac{\text{polylog } k}{e^{\log^2(k)}} = \frac{\text{polylog } k}{k^{\log k}}, \quad (\text{SM72})$$

where we use Cauchy–Schwarz inequality to reach (a) while (b) is due to $|f(x)| \leq C(1 + |x|^K)$ and $\mathbb{P}(|z| > \epsilon) \leq 2e^{-\epsilon^2/2}$ (Vershynin, 2018, Eq. (2.10)). Finally, we reach (c) by using moment bounds for $|z|$ from Lemma SM7. \square

Lemma SM11. Let $H_i(x)$ be the probabilist's i -th Hermite polynomial and $z_1, z_2 \stackrel{i.i.d.}{\sim} \mathcal{N}(0, 1)$. Then, for any $\rho \in [0, 1]$ and any $c \geq |\rho|$,

$$\mathbb{E}_{z_1, z_2} [H_i(\rho z_1 + \sqrt{c^2 - \rho^2} z_2) H_j(z_1)] = (i!) \rho^i \delta_{i,j}, \quad (\text{SM73})$$

where δ_{ij} is Kronecker delta function.

Proof. Let $a = (\rho/c)z_1 + \sqrt{1 - \rho^2/c^2}z_2$ and $b = z_1$. Observe that (a, b) is jointly Gaussian with $\mathbb{E}[a^2] = \mathbb{E}[b^2] = 1$ and $\mathbb{E}[ab] = (\rho/c)$. Furthermore, let $p(a, b)$ be the joint probability density function of (a, b) while $p(a)$ and $p(b)$ denoting the individual probability density functions. Using Mehler's formula Kibble (1945); Mehler (1866), we get

$$p(a, b) = p(a)p(b) \sum_{l=0}^{\infty} \frac{(\rho/c)^l}{l!} H_l(a) H_l(b). \quad (\text{SM74})$$

Then, it follows

$$\mathbb{E}_{z_1, z_2} [H_i(\rho z_1 + \sqrt{c^2 - \rho^2} z_2) H_j(z_1)] \quad (\text{SM75})$$

$$= \mathbb{E}_{a,b} [H_i(ca) H_j(b)], \quad (\text{SM76})$$

$$= \int_{-\infty}^{\infty} \int_{-\infty}^{\infty} H_i(ca) H_j(b) p(a, b) da db, \quad (\text{SM77})$$

$$= \int_{-\infty}^{\infty} \int_{-\infty}^{\infty} H_i(ca) H_j(b) p(a) p(b) \sum_{l=0}^{\infty} \frac{(\rho/c)^l}{l!} H_l(a) H_l(b) da db, \quad (\text{SM78})$$

$$= \sum_{l=0}^{\infty} \frac{(\rho/c)^l}{l!} \int_{-\infty}^{\infty} H_i(ca) H_l(a) p(a) da \int_{-\infty}^{\infty} H_j(b) H_l(b) p(b) db, \quad (\text{SM79})$$

$$= \sum_{l=0}^{\infty} \frac{(\rho/c)^l}{l!} \mathbb{E}_a [H_i(ca) H_l(a)] \mathbb{E}_b [H_j(b) H_l(b)], \quad (\text{SM80})$$

$$= \sum_{l=0}^{\infty} \frac{(\rho/c)^l}{l!} (i!)(j!)(c^i) \delta_{i,l} \delta_{j,l}, \quad (\text{SM81})$$

$$= (i!) \rho^i \delta_{ij}, \quad (\text{SM82})$$

where we use Lemma SM12 to reach the line before the last one. \square

Lemma SM12. Let $H_i(x)$ be the probabilist's i -th Hermite polynomial. Also, let $z \sim \mathcal{N}(0, 1)$. Then, for any $c \in \mathbb{R}$,

$$\mathbb{E}[H_i(cz) H_j(z)] = (i!)(c^i) \delta_{ij}. \quad (\text{SM83})$$

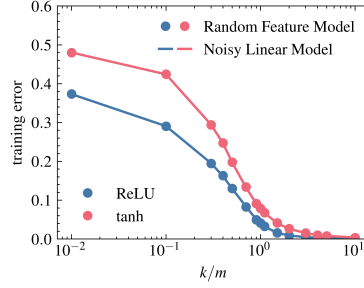


Figure SM1: Training errors for the misaligned case (the setting in Figure 1b)

Proof. It is known that $\mathbb{E}[H_i(z)H_j(z)] = (i!) \delta_{ij}$ (O’Donnell, 2014, Chapter 11.2). Here, we extend it to our case. For $i \neq j$, $\mathbb{E}[H_i(cz)H_j(z)] = 0$ by orthogonality. Let a_l be the coefficient of x^l in $H_i(x)$. Then, we have

$$\mathbb{E}[H_i(cz)H_i(z)] = \sum_{l=0}^i c^l \mathbb{E}[a_l z^l H_i(z)], \quad (\text{SM84})$$

$$\stackrel{(a)}{=} c^i \mathbb{E}[a_i z^i H_i(z)], \quad (\text{SM85})$$

$$\stackrel{(b)}{=} c^i \mathbb{E}[H_i(z)H_i(z)], \quad (\text{SM86})$$

$$\stackrel{(c)}{=} (i!)(c^i), \quad (\text{SM87})$$

where we use $\mathbb{E}[z^l H_i(z)] = \delta_{lj}$ due to orthogonality to reach (a) and (b) while (c) is because of $\mathbb{E}[H_i(z)H_i(z)] = (i!)$. Combining $i = j$ and $i \neq j$ cases, we get (SM83). \square

SM2 PLOTS FOR TRAINING ERRORS

For the sake of completeness, here, we provide the supplementary training error plots corresponding to the setting of Figure 1b and Figure 2 in Section 4.

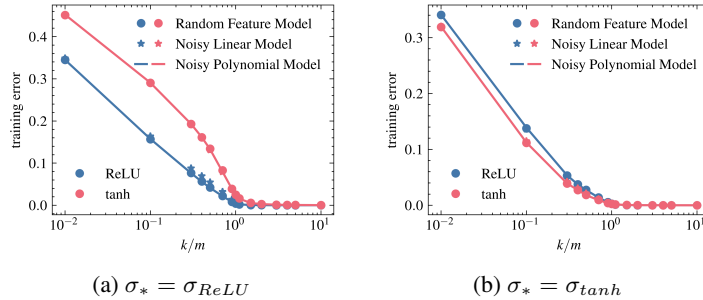


Figure SM2: Training errors for the aligned case (the setting in Figure 2).

SM3 DETAILS FOR CIFAR-10 EXPERIMENTS

In our experiments, we focus on binary classification between airplanes and automobiles using the CIFAR-10 dataset Krizhevsky et al. (2009) to demonstrate how our findings translate to real-world applications. We randomly select 2,000 samples from each class for training, while a separate set of 2,500 samples (distinct from the training set) is used to calculate the test (generalization) error. To prepare the input samples, we normalize the pixel values to achieve zero mean and unit variance for each color channel (R, G, B). Specifically, the pixel values are first scaled to the range [0, 1]

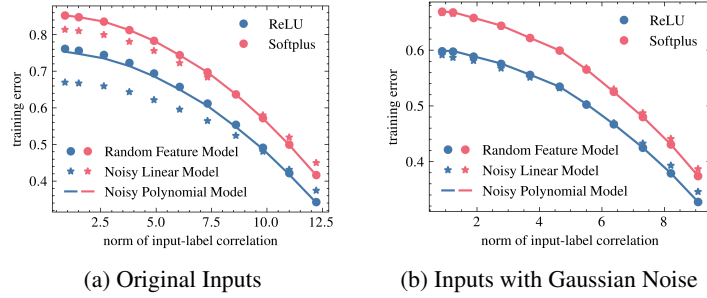


Figure SM3: Training errors for CIFAR-10 experiments (the setting in Figure 4).

by dividing by 255, followed by subtracting channel-wise means and dividing by their respective standard deviations. The images are then flattened into vectors for input into the model.

For the feature matrix \mathbf{F} , we sample entries independently from a normal distribution $\mathcal{N}(0, 1/\text{Tr}(\mathbb{E}[\mathbf{x}\mathbf{x}^T]))$, ensuring that $\mathbb{E}[(\mathbf{f}_i^T \mathbf{x})^2] = 1$ for all i , where \mathbf{f}_i denotes the i -th row of \mathbf{F} .

Our results are presented in two scenarios: first with the original normalized inputs (Figure 4a), and second after adding standard Gaussian noise (variance of one for each feature) to create a more isotropic covariance structure (Figure 4b). This addition of noise allows us to assess the performance equivalence between the linear model and RFM under conditions of weak input-label correlation.

For labels, we use $\{-1, 1\}$ for the first class and the second class, respectively. To control input-label correlation, we introduce a label flipping mechanism with probability p , where $p = 0$ corresponds to true labels (maximum correlation) and $p = 0.5$ represents random labels (minimum correlation). By varying p within the range $[0, 0.5]$, we interpolate between these two extremes and analyze how this affects model performance. The training errors for these experiments are illustrated in Figure SM3.